Efficient Tuning of Microstructure and Surface Chemistry of Nanocarbon Catalysts for Ethylbenzene Direct Dehydrogenation

Zhongkui Zhao, Yitao Dai, Guifang Ge, and Guiru Wang
State Key Laboratory of Fine Chemicals, Dept. of Catalysis Chemistry and Engineering, School of Chemical Engineering, Dalian University of Technology, Dalian 116024, P.R. China

DOI 10.1002/aic.14853
Published online May 7, 2015 in Wiley Online Library (wileyonlinelibrary.com)

A facile and scalable approach to efficiently tune microstructure and surface chemical properties of N-doped carbocatalysts through the controlled glucose hydrothermal treatment with diverse parameters and subsequent pyrolysis of pretreated carbonaceous materials with melamine (GHT-PCM) was presented. Various characterization techniques including high resolution transmission electron microscopy (HRTEM), N_2 adsorption desorption (BET), X-ray diffraction (XRD), X-ray photoelectron spectroscopy (XPS), Raman spectroscopy (Raman), and fourier transform infrared spectroscopy (FTIR) were employed to investigate the effect of prior GHT on the microstructure and surface chemical properties of N-doped carbocatalysts, as well as to reveal the relationship between catalyst nature and catalytic performance in oxidant- and steam-free direct dehydrogenation (DDH) of ethylbenzene for styrene production. It was found that the GHT process and its conditions significantly affect microstructure and surface chemical properties of the N-doped carbocatalysts, which subsequently influences their catalytic performance in DDH reaction dramatically. Interestingly, the prior GHT can remove the carbon nitride layer formed on parent nanocarbon in the process of melamine pyrolysis, produce structural defects, and tune surface element component, through the "detonation" of polysaccharide coating on nanocarbon. The as-prepared N-doped CNT (M-Glu-CNT) by the established GHT-PCM approach demonstrates higher catalytic performance (4.6 mmol $g^{-1}h^{-1}$ styrene rate with 98% selectivity) to the common N-doped CNT (M-CNT, 3.4 mmol g^{-1} h^{-1} styrene rate with 98.2% selectivity) as well as to pristine CNT (2.8 mmol g^{-1} h^{-1} styrene rate with 96.8% selectivity), mainly ascribed to increased structural defects, enriched surface ketonic C═O groups, and improved basic properties from N-doping on the M-Glu-CNT, those strongly depend on GHT conditions. The excellent catalytic performance of the developed M-Glu-CNT catalyst endows it with great potential for future clean production of styrene via oxidant- and steam-free conditions. Moreover, the directed GHT-PCM strategy can be extended to the other N-doped carbonaceous materials with enhanced catalytic performance in diverse reactions by tuning their microstructure and surface chemistry. © 2015 American Institute of Chemical Engineers *AIChE J*, 61: 2543–2561, 2015
Keywords: dehydrogenation, carbocatalyst, microstructure and surface chemistry, glucose hydrothermal pretreatment, heterogeneous catalysis

Introduction

Owing to the broad availability, good environmental acceptability, high corrosion resistance, and unique surface properties, nanocarbon materials have been demonstrated to be promising and sustainable low-cost metal-free alternatives to metal-based catalysts for diverse organic reactions.[1–8] Especially, based on their unique physical and chemical properties, N-doped carbonaceous materials including N-doped graphene, carbon nanotube, fullerene, carbon nanosphere, diamond, nanofiber, nanosheet, carbon dot, porous carbon, and their composites have been extensively applied to diverse fields including catalysis (thermalcatalysis, photocatalysis, and electrocatalysis),[9–16] nanoelectronics and photonics,[17–19] Solar cells,[20,21] sensors,[22,23] lithium/sodium ion battery,[24,25] supercapacitors,[26,27] CO_2 capture,[28,29] and so on. The N-containing heteroatoms modification respents one of the largest domains related to nanostructued carbonaceous materials.[30,31] The N-doped carbon materials can be synthesized by two differnt methods: direct synthesis and post-treatment. The former may have potential to fabricate homogeneous heteroatoms-doped materials, but the fabrication of N-doped carbon nanostructures with diverse morphologies via direct synthesis still remains a challenge. However, the post-treatment may be considered as a facile approach for synthesizing many N-doped nanostructured carbonaceous materials like N-doped graphene, carbon nanotube, fullerene, nanofiber, and so forth.[1–29] Post-treatment includes thermal treatment, plasma treatment, and N_2H_4 treatment.[13] Thermal treatment refers to the method of heating carbon nanostrctures in NH_3 atmosphere or pyrolysis of carbon materials with N-containing precursors to produce N-doped nanostructured carbon materials,[13,30,31]

Correspondence concerning this article should be addressed to Z. K. Zhao at zkzhao@dlut.edu.cn.

Scheme 1. Illustration of synthetic procedure for novel carbon nitride materials with tunable microstructure and surface chemical properties (M-Glu-CNT or M-Glu-CMK-3) through a facile and scalable mechanical milling and subsequent pyrolysis approach of the glucose hydrothermally pretreated carbonceous materials like CNT or CMK-3 with melamine.

[Color figure can be viewed in the online issue, which is available at wileyonlinelibrary.com.]

which has been consider to be a facile, scalable, and generally used method to prepare N-doped carbon materials. Moreover, the N-incorporation into carbon matrix entirely takes place on the surface of carbon nanostructures by the post-thermal treatment, where the reactions happen. Therefore, the post-treatment by heating is a robust strategy to prepare metal-free carbocatalysts.[9–16]

Owing to high toxicity and strong corrosiveness of NH_3, the pyrolysis of carbon materials with diverse N-containing precursors like melamine, pyridine, urea, and so forth was an extensively adopted method.[30–34] Furthermore, the pyrolysis of carbon materials with such solid N sources like melamine can lead to more structural defects,[35] which is favorable for absorbing and activating reactants, and therefore, improves the catalytic performance of carbocatalysts.[36–38] Conversely, this kind of pyrolysis method has its inherent disadvantage: high temperature resulting in low doping level due to cutting C—N bonds at such as high temperature, but low pyrolysis temperature would lead to thicker CNx layer coating on carbon nanostructures, which may deteriorate their catalysis by inhibiting surface active sites from reactants.[32,39] To achieve highly active carbocatalysts, it is highly desirable to create surface CNx layer-free N-doped carbonaceous nanostructures with higher N-doping level at a little lower pyrolysis temperature.

In this work, we first present a controlled glucose hydrothermal treatment and subsequent pyrolysis of pretreated carbonaceous materials with melamine (GHT-PCM) strategy (Scheme 1) to prepare N-doped CNT (M-Glu-CNT), through which the microstructure and surface chemical properties can be efficiently tuned. In this process, the pristine CNT was hydrothermally pretreated by glucose aqueous solution, and then the pretreated CNT was finely ground with melamine and followed by pyrolysis at 750°C in N_2 atmosphere. Interestingly, the prior GHT can remove the carbon nitride layer on CNT formed by pyrolysis of melamine, simultaneously produce structural defects as well as tune surface chemical component, through the controllable "detonation" of polysaccharide coating on CNT surface by GHT approach in the pyrolysis procedure. However, there are thick CNx layers coating on N-doped nanostructured CNT (M-CNT) prepared only by pyrolysis but without the prior GHT treatment. Moreover, the created and increased structural defects on the surface of nanocarbons may promote their catalytic performance.[36–38]

Direct dehydrogenation (DDH) of ethylbenzene to styrene is one of the commercially important reactions in chemical industry. The commonly used catalyst is K-Fe; however, it must be noticed that steam is used as excess molar amount with respect to ethylbenzene (about 2-3:1 for current technology); the amount of spent energy is relatively high.[40–42] Developing a robust catalyst with high coke-resistance under low ratio of steam to styrene even under steam-free conditions is highly desirable. The DDH reaction of ethylbenzene to styrene under oxygen- and steam-free conditions was reported using nanodiamond as an efficient metal-free catalyst,[43] which inspires many researchers to develop carbon-based catalysts for this reaction. However, so far, the further increase in catalytic activity is required. We previously demonstrated that N-doping can efficiently improve the catalytic performance of carbon materials.[39,44,45] Recently, it was reported that, besides the established ketonic C═O, the structural defects are also the active sites for DDH of hydrocarbons.[46–48] Therefore, we envision that the catalytic properties of carbon nanotube can be hopefully improved by N-doping and defect formation. This may result in an excellent catalyst for DDH reaction. Various characterization techniques including high resolution transmission electron microscopy (HRTEM), X-ray diffraction (XRD), X-ray photoelectron spectroscopy (XPS), Raman spectroscopy (Raman),

and fourier transform infrared spectroscopy (FTIR) were employed to reveal the effect of prior GHT on the microstructure and surface chemical properties of N-doped carbonaceous materials. DDH reaction of ethylbenzene to styrene was used as a model reaction to investigate the promoting effect of GHT pretreatment on the catalytic performance. The optimized M-Glu-CNT demonstrates 1.35 and 1.64 times the steady-state styrene rate of the M-CNT prepared without GHT treatment and the pristine CNT, respectively. Correlated the reaction results to the carbon materials nature, the structure-performance relationship for DDH reaction was revealed. The superior catalytic performance of the developed M-Glu-CNT catalyst in this work can be ascribed to increased structural defects, decreased size of in-plane crystallites, enriched surface C═O group, and improved basic properties by the promoting N-doping on the M-Glu-CNT by surface hydroxyl groups from GHT. The directed prior controlled GHT and subsequently pyrolysis approach can be extended to the other N-doped carbonaceous materials.

Experimental Section

Synthesis of mesoporous silica SBA-15

SBA-15 was prepared according to the procedure reported by Zhao et al.[49,50] In a typical synthesis, 4.0 g of Pluronic P123 purchased from Sigma-Aldrich Co. was dissolved in 30 g of deionized water and 120 g of 2 M HCl solution with stirring at 35°C. Then, 8.50 g of TEOS was added into the above solution with stirring at 35°C for 20 h. The resulting mixture was aged at 80°C overnight. The obtained solid product was recovered, washed, and then dried at room temperature. The final product was calcined at 500°C for 6 h.

Synthesis of mesoporous carbon CMK-3

According to Ref. 51, CMK-3 was also prepared. Briefly, 1 g of calcined SBA-15 was added to a solution containing 1.25 g of sucrose, 0.14 g of H_2SO_4, and 5 g of H_2O. The mixture was placed in a drying oven at 100°C for 6 h, and then the temperature was increased up to 160°C and kept this temperature for 6 h. The resultant solid, containing silica template, partially polymerized and carbonized sucrose, was treated again at 100°C, and then at 160°C using the same drying oven after the addition of the solution containing 0.8 g of sucrose, 0.09 g of H_2SO_4, and 5 g of H_2O. The carbonization was performed by pyrolysis at 900°C in nitrogen atmosphere. The obtained carbon-silica composite was washed with 5 wt % HF at room temperature to remove the silica template. The silica template-free carbon product was obtained by filtering, then washing with ethanol, and finally drying at 120°C overnight.

Glucose hydrothermal pretreatment of multiwalled CNT and CMK-3

Typically, the pristine multiwalled CNT (purity $>$ 95%, outer diameter $<$ 8 nm, with a length of 10–30 μm) purchased from Chengdu Organic Chemicals Co., Chinese Academy of Sciences was dispersed in the 16.7 wt % glucose aqueous solution. The suspension was transferred into a 50-mL Teflon-lined hydrothermal autoclave and then maintained at 100–140°C for 10–40 h. After the hydrothermal procedure, the mixture was filtered and washed with deionized water and then with ethanol, followed by drying at about 100°C overnight. Then, the hydrothermally pretreated multiwalled CNT was obtained, which is denoted as Glu-CNT-0. By changing hydrothermal conditions including glucose concentration, hydrothermal temperature, and hydrothermal time, a series of glucose hydrothermally treated CNTs were obtained. Using the same procedure, the glucose hydrothermal pretreated CMK-3 (Glu-CMK-3) was also prepared.

Pyrolysis procedure of carbonaceous materials with melamine

Typically, the prior glucose hydrothermal-treated Glu-CNT-0 was finely ground with melamine in an agate mortar (1:30) and then heated up to the desired temperature in N_2 atmosphere for pyrolysis process at the established ramp rate to obtain the final N-CNT (Scheme 1), and it is denoted as M-Glu-CNT. Using the different CNTs pretreated by different glucose concentrations (9.1, 16.7, and 28.6 wt %), various hydrothermal temperature (100, 120, and 140°C), and diverse hydrothermal time (10, 20, and 40 h), a series of novel N-doped CNTs were prepared, which are named as M-Glu-CNT-9.1%, M-Glu-CNT-16.7%, M-Glu-CNT-28.6%, M-Glu-CNT-100, M-Glu-CNT-120, M-Glu-CNT-140, M-Glu-CNT-10, M-Glu-CNT-20, and M-Glu-CNT-40, respectively. The common N-doped CNT prepared by the pyrolysis of pristine CNT and melamine but without glucose hydrothermal pretreatment was also prepared and labeled as M-CNT. To find out whether the presented GHT-PCM strategy can be efficiently extended to the other N-doped carbonaceous materials, the novel N-doped CMK-3 was also prepared by pyrolysis of Glu-CMK-3 and melamine. The as-prepared N-doped mesoporous carbon is denoted as M-Glu-CMK-3.

Characterization of samples

X-ray diffraction (XRD) patterns were collected from 10 to 80° at a step width of 0.02° using Rigaku Automatic x-ray Diffractometer (D/Max 2400) equipped with a CuKa source ($\lambda = 1.5406$ Å). Transmission electron microscopy (TEM) images were obtained using Tecnai F30 HRTEM instrument (FEI Corp.) at an acceleration voltage of 300 kV. The XPS spectra were carried out on an ESCALAB 250 XPS system with a monochromatized Al Ka x-ray source (15 kV, 150 W, 500 μm, pass energy = 50 eV). The Raman spectra were measured using a laser with an excitation wavelength of 532 nm at room temperature on a Thermo Scientific DXR Raman microscope. FTIR spectroscopy characterization of samples was performed at 50°C under ultrahigh vacuum using a Bruker EQUINOX55 infrared spectrometer. Nitrogen adsorption and desorption isotherms were determined on a Beishide apparatus of model 3H-2000PS1 system at −196°C. The specific surface areas were calculated by the N2 adsorption desorption (BET) method as well as the micropore and mesopore size distributions were calculated from adsorption branch of the isotherm by H-K and BJH model, respectively.

Catalytic performance measurement

DDH of ethylbenzene, as model reaction, was carried out at 550°C for 20 h in a stainless steel, fixed bed flow microreactor. Typically, 25 mg catalyst was placed at the center of the reactor between two quartz wool plugs. The system was heated to 600°C and kept for 30 min in Ar for pretreatment of catalyst. After the system was cooled down to 550°C and kept for 10 min, the reactant of 2.8% ethylbenzene with feed flow rate 10 mL min^{-1} and Ar as balance was then fed into the reactor from a saturator kept at 40°C at atmospheric pressure. The

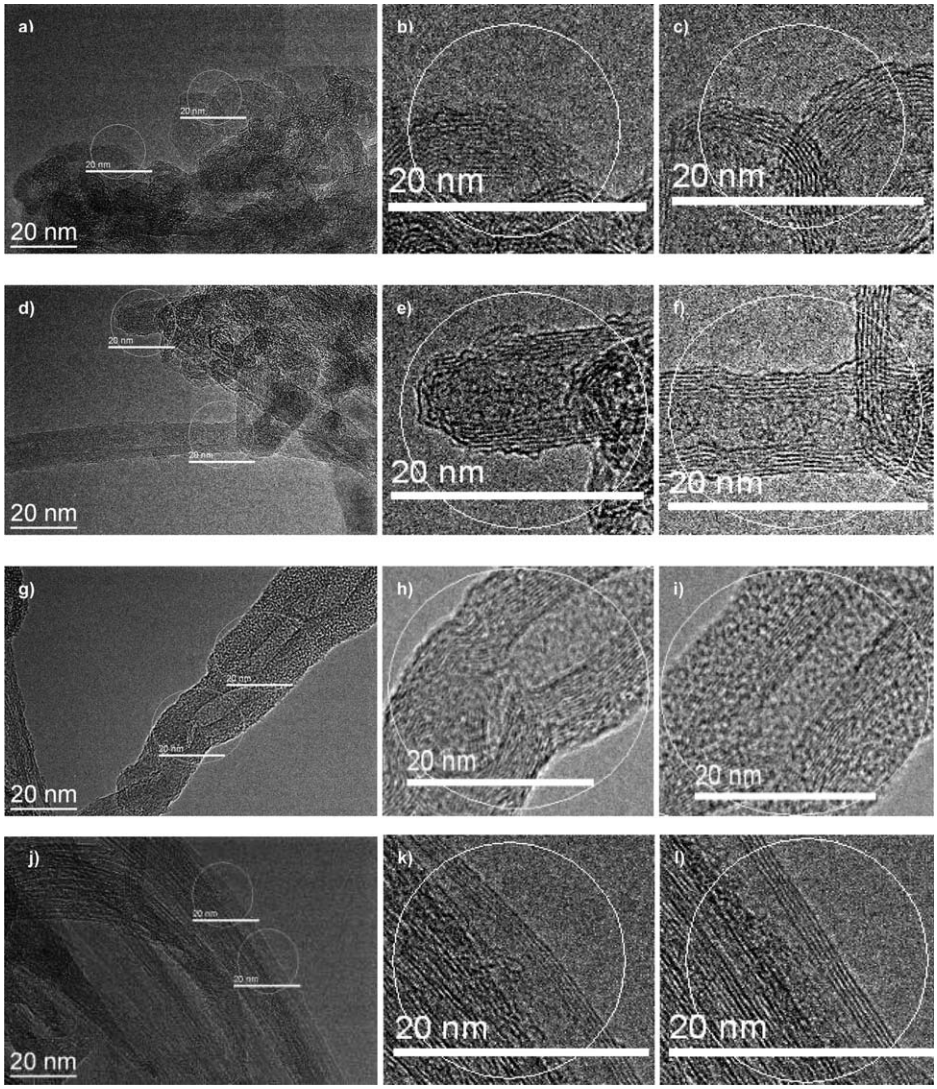

Figure 1. HRTEM images of (a–c) M-Glu-CNT, (d–f) Glu-CNT, (g–i) M-CNT, and (j–l) the pristine CNT samples.

effluent from the reactor was condensed and absorbed in two traps containing certain amount of ethanol connected in a series. The condensed material was cooled externally in an ice water bath. Quantitative analysis of the collected reaction products (ethylbenzene, styrene, toluene, and benzene) was performed on a FULI 9790 II GC equipped with HP-5 column, 30 m $\times$ 0.32 mm $\times$ 0.25 μm, and FID detector. The resulting carbon balance was above 100 $\pm$ 4% in all reactions (Calculation method: the percentage of actually measured carbon atom number for the unreacted ethylbenzene, produced styrene, and the side products benzene and toluene per hour by internal standard method to the carbon atom number of ethylbenzene flowing through the reactor per hour; the same measurement process as above was performed five times). The styrene rate and selectivity of styrene are employed to compare the catalytic performance of the fabricated catalysts for DDH reaction. The styrene rate is calculated as the formed styrene molar amount per gram catalyst per hour, and the selectivity of styrene is denoted as the percentage of the desired styrene to the total products including the desired styrene and the by-products that containing benzene and toluene. The steady-state rate and selectivity are employed as the index for evaluating the developed catalysts. Catalytic performance measurements over series of N-doped CNTs and mesoporous carbon prepared by the developed GHT-PCM approach (M-Glu-CNT-9.1%, M-Glu-CNT-16.7%, M-Glu-CNT-28.6%, M-Glu-CNT-100, M-Glu-CNT-120, M-Glu-CNT-140, M-Glu-CNT-10, M-Glu-CNT-20, and M-Glu-CNT-40, M-Glu-CMK-3) and the common N-doped carbonaceous materials (M-CNT and M-CMK-3) were performed. For comparison, the catalytic properties of the pristine CNT, Glu-CNT (was obtained by the annealing of Glu-CNT-0 under the same conditions as those for pyrolysis procedure but in the absence of melamine).

Results and Discussion

Effect of glucose hydrothermal pretreatment

Figure 1 presents the typical HRTEM images of M-Glu-CNT, M-CNT, Glu-CNT, and pristine CNT samples. In comparison with pristine CNT (Figures 1j–l), the visible CNx layer on the M-CNT prepared by pyrolysis of pristine CNT and melamine can be observed (Figures 1g–i). The presence of N element on this sample has been confirmed by the following XPS experiment, and the CNx can be produced by the pyrolysis of melamine. However, no CNx layer on the M-Glu-CNT sample can be observed (Figures 1a–c),

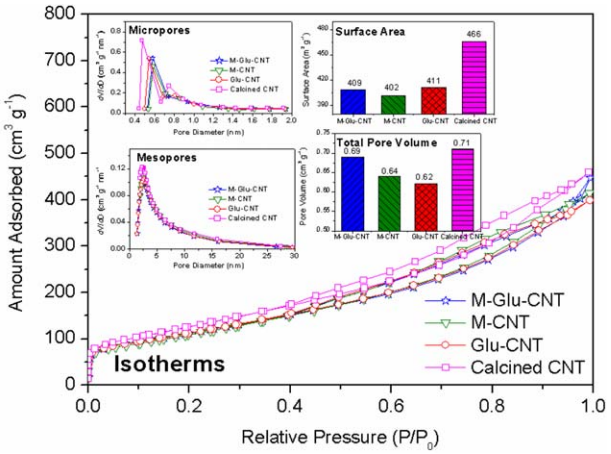

Figure 2. Nitrogen adsorption–desorption isotherms of the M-Glu-CNT, Glu-CNT, M-CNT, and the calcined CNT samples. Insets: Barrett–Joyner–Halenda adsorption mesopore size distribution, Horvath–Kawazoe adsorption micropore size distribution, and specific surface area.

[Color figure can be viewed in the online issue, which is available at wileyonlinelibrary.com.]

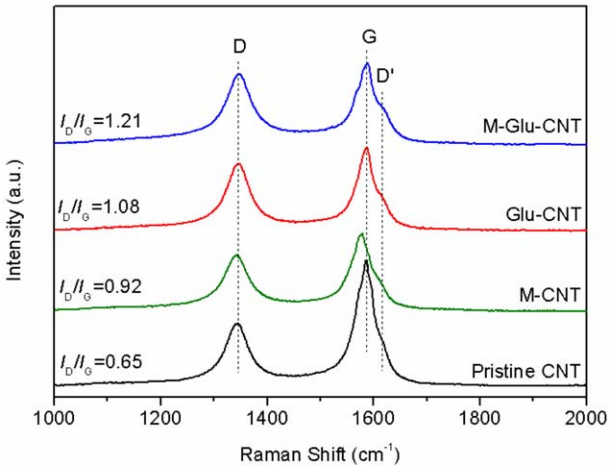

Figure 3. Raman spectra of M-Glu-CNT, Glu-CNT, M-CNT, and the pristine CNT samples.

[Color figure can be viewed in the online issue, which is available at wileyonlinelibrary.com.]

although the existence of N element on the surface of this sample identified by XPS analysis. Interestingly, we can clearly see the enhanced structural defectiveness on both M-Glu-CNT prepared by pyrolysis of GHT pretreated CNT in the presence of melamine and Glu-CNT (Figures 1d–f) by annealing process of GHT pretreated CNT without melamine at the same pyrolysis temperature. In comparison with M-CNT, the disappearance of CNx and the formation of surface structural defects on the M-Glu-CNT may be resulted from the explosive decomposition of coated polysaccharide on CNT produced by glucose polymerization in the GHT process.[52,53] It was previously demonstrated that the maximum structural defectiveness promoted diverse catalytic reations,[36–38] also the DDH of propane on annealed nanodiamond.[46] We envisioned that the created or enhanced structural defectiveness on M-Glu-CNT sample by GHT-PCM approach (also called as glucose hydrothermal preptreatment assisted pyrolysis of CNT with melamine) may improve the catalytic performance of the N-doped CNT in DDH reaction of ethylbenzene. This has been confirmed by the following reaction results in this work.

As shown in Figure 2, the microstructure and macrostructure have been changed due to the treatments. Especially, the lowest surface area on M-CNT can be observed, ascribed to the CNx layer or carbon fragment covering on CNT as confirmed by HRTEM. The surface area rankings of the three modified CNT is Glu-CNT > M-Glu-CNT > M-CNT, suggetsing that the glucose hydrothermal process may inhibit the decrease in surafce area caused by the CNx layer or carbon fragment covering on CNT through the explosive decomposition of polysaccharide. This is in consistent with results obtained from HRTEM. The high surface area and pore volume can favor the accessibility of active sites to reactants, and therefore, enhances the catalytic reaction.

As shown in Figure 3, Raman peaks appear at around 1337 and 1585 cm^{-1} on the four samples assigned to D and G peaks can be observed, which correspond to A1g mode in disorder carbon or surface structural defects and to E2g mode for ideal graphitic carbon, respectively. The larger I_D/I_G of M-Glu-CNT than that of Glu-CNT, as well as larger I_D/I_G of M-CNT than that of pristine CNT can be observed, indicating more structural defects, disordered carbon, and lattice edge produced by N-doping.[34,54,55] Interestingly, more structural defect, disordered carbon, and lattice edge on the Glu-CNT and M-Glu-CNT in comparison of pristine CNT and M-CNT can be observed, which demonstrates the effect of prior GHT before pyrolysis process. Besides, the intensified D′ peak appears as a shoulder peak of G-band on M-Glu-CNT sample in comparison with that of M-CNT, implying the enhanced structural defectiveness,[56] which agrees with the results from HRTEM experiments. Furthermore, the larger I_D/I_G for M-Glu-CNT in comparison to that for M-CNT also indicates the smaller in-plane crystallite size of M-Glu-CNT prepared by GHT-PCM approach to M-CNT by pyrolysis of pristine CNT and melamine without GHT process.[34,54] Also, we can see a shift to lower wavenumber toward G-peak on M-CNT in comparison that of the other samples, which may be due to the different surface carbon structure (CNx layer from melamine pyrolysis). This is consistent with the results from the HRTEM. All in all, the intensified structural defectiveness on the surface of M-Glu-CMT can be obtained by the explosive decomposition of formed polysaccharide in the GHT process of pristine CNT, identified by HRTEM and Raman characterization results. The intensified surface structural defectiveness may promote the catalysis of the samples for diverse reactions including but not limited to DDH reaction.

The structure of the developed M-Glu-CNT, Glu-CNT, M-CNT, the calcined CNT and the pristine CNT was further investigated by XRD analysis. From Figure 4, the strong diffraction peaks at around 26°, 43.3°, 44.6° corresponding to (002), (100), (111) planes on M-Glu-CNT, Glu-CNT, calcined CNT, and pristine CNT can be clearly resolved, indicating the well-formed graphitic carbon structure.[39,44] However, weak peak toward (002) plane and no peaks corresponding to (100) and (111) facets on the M-CNT can be observed. This suggests the existence of CNx layer on M-CNT, identified by the HRTEM and the XPS data. By carefully comparing the peaks for (002) plane, the GHT leads to

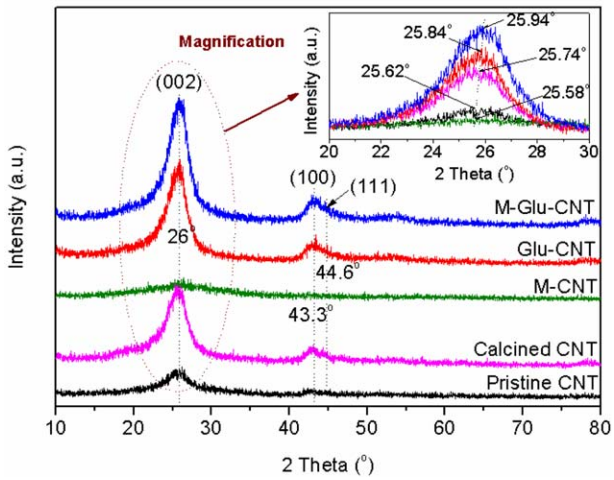

Figure 4. XRD patterns of M-Glu-CNT, Glu-CNT, M-CNT, as well as the pristine and calcined CNT samples.

[Color figure can be viewed in the online issue, which is available at wileyonlinelibrary.com.]

XRD peak shifting from 25.58° (M-CNT) to 25.94° (M-Glu-CNT), which corresponds to the 0.343 nm of d-spacing for M-CNT and 0.348 nm for M-Glu-CNT. The value for M-Glu-CNT is larger than that for pristine graphite (0.34 nm) as the result of swelling of graphitic sheets produced by the release of oxygenated functional groups.[57] The much stronger XRD peak for M-Glu-CNT than that for M-CNT suggests the higher graphitization led by the GHT process. However, as for the Raman results for M-Glu-CNT and M-CNT, the 1.21 of much higher I_D/I_G value for the former than that (0.92) for the latter can be clearly observed. Correlated to Raman results to XRD patterns, the more disordered carbon on M-Glu-CNT can be ruled out, and the higher I_D/I_G value for Raman spectra of M-Glu-CNT should be ascribed to more structural defects and lattice edge produced by the possible explosive decomposition of polysaccharide. It was demonstrated that the defects also can activate the C—H bond of alkanes,[46] the enriched surface defective sites on the M-Glu-CNT may allow it to be a highly active catalyst for DDH reaction.

The catalytic performance of carbocatalysts is significantly dependent on their microstructure especially surface microstructure and surface chemical properties.[2,44,58,59] Herein, the XPS analysis on M-Glu-CNT and M-CNT was carried out to investigate the surface chemical properties corresponding to the nature and coordination of the carbon, nitrogen, and oxygen for the samples. The Glu-CNT-0 (prepared by the same process as that for M-Glu-CNT except for the absence of melamine) and pristine CNT are also included for comparison. The XPS spectra and quantitative analysis results are presented in Figure 5,9 and Table 1, 2 respectively.

The XPS survey spectra of the M-Glu-CNT, Glu-CNT, M-CNT, and pristine CNT presented in Figure 5a show that the C, N, and O elements appear on M-CNT and M-Glu-CNT, and only C and O on Glu-CNT and pristine CNT samples. From Table 1, 1.8 and 1.9 At % of N element on M-CNT and M-Glu-CNT, respectively, is shown. Generally, the explosive decomposition of polysaccharide can lead to a decrease in N-doping level, and even can lead to the decomposition of formed CNx layer from melamine and the formation of structural defects identified by above characterization results. However, the explosive decomposition does not lead to a decrease in N atom content on N-doped CNT sample (M-Glu-CNT). On the contrary, a slight higher N content on M-Glu-CNT than that on M-CNT can be obtained. In our opinion, the explosive decomposition of polysaccharide may lower the N-doping level, but the hydrogen bond effect between melamine and the hydroxyl groups of polysaccharide can increase the N-doping level. From Table 1, the decreased surface O content on the M-CNT (1.6 At %) in comparison with pristine CNT (4.1 At %) results from the O release in the pyrolysis process at high temperature. However, the 4.2 At % of O content on the Glu-CNT sample can be observed although it suffered from the same annealing process. The increased O content may be caused by the polysaccharide on the CNT formed by the GHT process or the more defect sites anchored O-containing species.[46] Furthermore, the 7.4 At % of the higher O content on M-Glu-CNT than that of the others, and even than Glu-CNT is seen. This is possibly resulted from the formed polysaccharide on the CNT, the inhibition of O release by the presence of melamine, and the anchored O-containing species on defect sites. The C 1s peak region in the XPS spectra of the M-Glu-CNT and M-CNT samples (Figure 5b and Table 1) was deconvoluted to five peaks at around 284.6, 285.2, 286.0, 287.0, and 288.1–288.3 eV corresponding to C═C, C—N, C—C, C—O, and C═O/C═N, respectively.[2,34,54–61] The presence of C—N and/or C═N peaks indicates the N incorporation into carbon matrix. The N 1s XPS peak (Figure 5c and Table 1) illustrates that the N atoms in M-Glu-CNT and M-CNT have been doped into the graphene lattice in a form of "pyridinic N," "pyrrolic N," graphitic N, and oxidized N, which appear at around 398.6, 400.2, and 401.5, 404.0–404.9 eV, respectively.[34,60–63] This suggests the N incorporating but not absorbing on the materials surface.

Table 1. XPS Quantitative Analysis Results for M-Glu-CNT, Glu-CNT, M-CNT, and CNT Samples

Sample	C-1[a] (%)	C-2[a] (%)	C-3[a] (%)	C-4[a] (%)	C-5[a] (%)	N[b] (%)	N-1[c] (%)	N-2[c] (%)	N-3[c] (%)	N-4[c] (%)	O[d] (%)	O-1[e] (%)	O-2[e] (%)	O-3[e] (%)
CNT	77.7	–	10.4	5.3	6.5	–	–	–	–	–	4.1	15.8	47.8	36.4
M-CNT	58.4	19.5	10.8	5.3	5.9	1.8	50.1	27.9	14.2	7.8	1.6	31.2	58.8	10.0
Glu-CNT	78.2	–	12.8	4.3	4.7	–	–	–	–	–	4.2	6.7	53.5	39.8
M-Glu-CNT	70.3	7.5	14.2	2.3	5.7	1.9	43.1	34.2	11.9	10.8	7.4	10.0	56.5	33.5

[a]Percentage of various nitrogen species occupying in the total C content; C-1, C-2, C-3, C-4, and C-5 are denoted as C═C, C—N, C—C/C—O, C═O/C═N, and O—C═O, respectively.
[b]The surface N content of the materials from XPS.
[c]Percentage of various nitrogen species occupying in the total N content; N-1, N-2, N-3, and N-4 are denoted as pyridinic N, pyrrolic N, graphitic N, and oxidized N, respectively.
[d]The O atom molar percentage on the material surface from XPS analysis.
[e]Percentage of various nitrogen species occupying in the total O content; O-1, O-2, and O-3 are denoted as C═O, O═C—O, and C—OH/C—O—C, respectively.

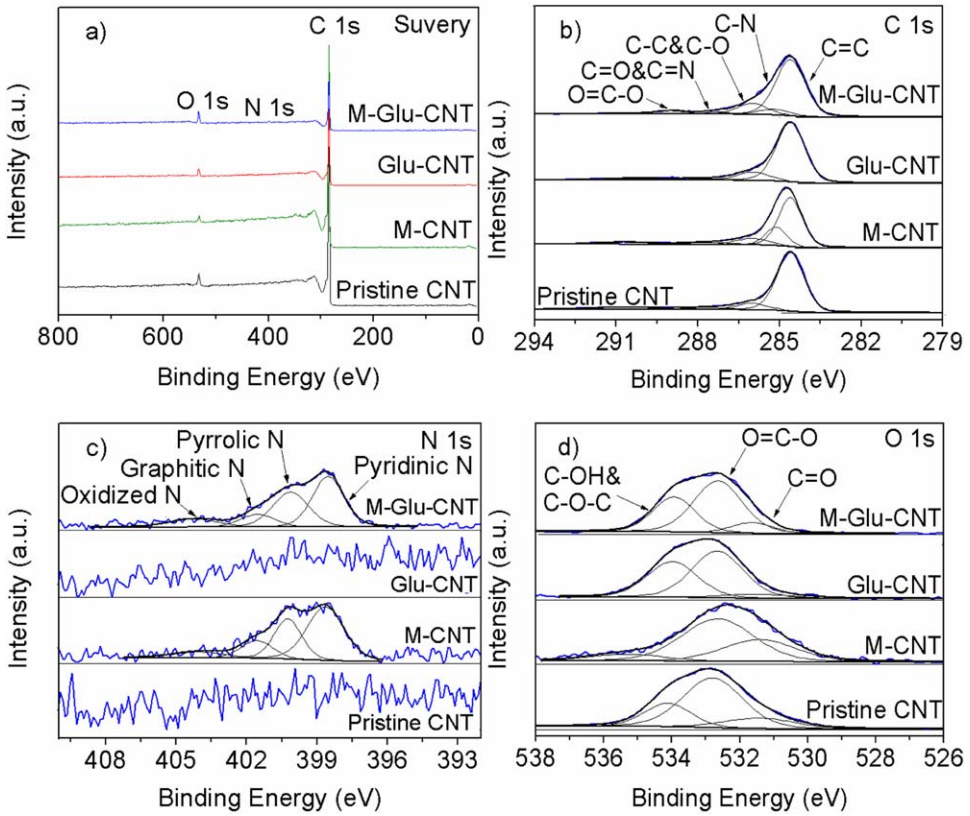

Figure 5. XPS spectra of M-Glu-CNT, Glu-CNT, M-CNT, and the pristine CNT samples. (a) Suvery spectra; (b–d) C 1s, N 1s, and O 1s, respectively.

[Color figure can be viewed in the online issue, which is available at wileyonlinelibrary.com.]

Furthermore, from Table 1, the more pyrrolic N and oxidized N species on the M-Glu-CNT than those on M-CNT can be observed, which may be one of the reasons for superior catalytic performance of G-M-CNT in DDH reaction. The main side-products for the catalytic DDH of ethylbenzene are benzene and toluene produced by the cracking of ethylbenzene, which is consistent with the results reported in literatures.[39,43,44,46] The surface phenolic hydroxyl group and/or possible COOH may promote the cracking of ethylbenzene due to its acidity, as acid sites are active for cracking reaction of hydrocarbon.[64] The incorporated N atom into carbon matrix can increase the electron density of carbon materials, and therefore, strengthens the basic properties but weakens the acidity of the catalyst, which may result in an improvement in catalytic activity for styrene production and simultaneously compressing the benzene and toluene formation.[39,43,46] The O 1s XPS spectra can be deconvoluted into three peaks with the binding energies at around 531.5, 532.6, and 538.8–535.3 eV, assigned to C═O, O═C—O, and C—O—C/C—OH containing groups, respectively (Figure 5d and Table 1).[65] From Table 1, the surface O content on the CNT, M-CNT, Glu-CNT, and M-Glu-CNT is 4.1, 1.6, 4.2, and 7.4 At %, respectively. The pyrolysis procedure and CNx coating leads to the decreasing surface O content on M-CNT in comparison to that on CNT. However, the prior GHT process leads to a significant increase in surface O content on M-Glu-CNT in comparison to that on M-CNT. Besides the defect sites,[46] the surface ketone-type C═O content of the following materials, CNT, M-CNT, Glu-CNT, and M-Glu-CNT is 0.65, 0.50, 0.28, and 0.74%, respectively. N-doping by pyrolysis of glucose hydrothermal-treated CNT and melamine may increase the catalytic active sites amount, and therefore, significantly improved the catalytic performance in DDH reaction.

From the above characterization results for the microstructure and surface chemistry, the GHT approach before pyrolysis for preparing N-doped CNT can lead to the disappearance of CNx layer formed by melamine pyrolysis and the enhanced surface defectiveness by explosive decomposition of polysaccharide, as well as can enrich surface N (possibly through the hydrogen-bond effect between melamine and hydroxyl groups of polysaccharide) and O contents. To further confirm the formation of polysaccharide on CNT and also to probe why the GHT has significant effect on material feature and the catalysis of N-doped CNT, the HRTEM, Raman, FTIR, XPS experiments (Figures 6–9) were performed on the Glu-CNT-0 (glucose hydrothermal pretreated CNT, used as parent carbon nanostructured material for preparing M-Glu-CNT by pyrolysis) and pristine CNT.

From Figures 6a–c, the carbon fragments coating on the CNT for Glu-CNT-0 can be observed, suggesting the formation of polysccharide by GHT process. However, clean surface for pristine (Figures 6d–f) is seen. Moreover, the carbon fragments are quitely different from the CNx layer formed by pyrolysis of melamine on the M-CNT sample (Figures 1g–i). From Figure 7, the significantly different Raman spectra between Glu-CNT-0 and pristine CNT further indicate the different surface feature between Glu-CNT-0 and pristine CNT. By comparing FTIR spectra of Glu-CNT-0 and pristine CNT (Figure 8), the much stronger peaks corresponding to C═O and C—OH/C—O—C at around 1703 and 1184 cm^{-1}, respectively, on Glu-CNT-0 than those on

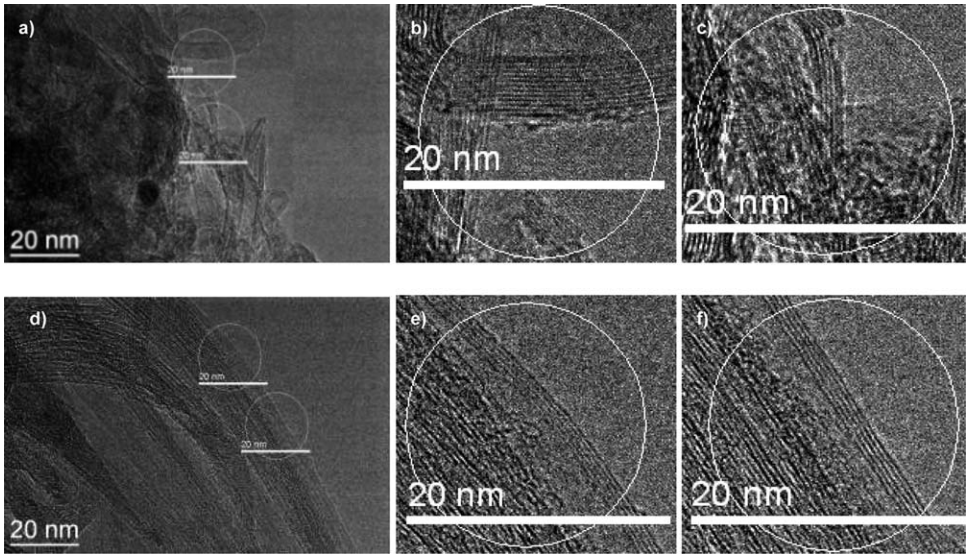

Figure 6. HRTEM images of (a–c) Glu-CNT-0 and (d–f) pristine CNT samples.

pristine CNT can be observed, further demonstrating the existence of polysccharide coating CNT on the Glu-CNT sample. From Figure 9 and Table 2, the increase in surface O atom on the Glu-CNT-0 in comparison with pristine CNT is another proof for the existing polysaccharide, which is consistent with the results from HRTEM, Raman spectra, and FTIR spectra.

Oxidant- and steam-free DDH of ethylbenzene catalyzed by metal-free carbocatalysts has been considered as sustainable and robust strategy for the styrene production.[39,43,44] Herein, the catalytic performance of the developed samples for DDH reaction of ethylbenzene was performed. Figure 10 presents the reaction results for DDH reaction over M-Glu-CNT, Glu-CNT, M-CNT, and pristine CNT. From Figure 10, the steep decline of catalytic activity initially for all samples can be observed, and is consistent with the reported results for the DDH reaction catalyzed by carbocatalysts.[39,43,44] The rapid decrease in activity at the initial period may ascribed to the hydrogen passivation.[2] The initial activity decreases, but reaches steady state at about 15–20 h of time on stream.[44] In this work, the steady-state rate was used as an index to compare the catalytic activity of the diverse samples, and the focus was put into the effect of glucose hydrothermal pretreatment and the GHT conditions on the steady-state rate. The N-doped CNTs including M-Glu-CNT and M-CNT show superior catalytic activity and slight higher selectivity to the undoped CNT and Glu-CNT, ascribed to the N-doping as well as the produced defect and increased surface ketone-type C═O amount on samples resulted from N-doping, confirmed by HRTEM, Raman, and XPS results.[39,44] Moreover, we can see the Glu-CNT shows slight higher catalytic activity than the pristine CNT. However, XPS results demonstrate the Glu-CNT has lower surface C═O content. From HRTEM and Raman spectra, the intensified structural defectiveness on the Glu-CNT in comparison with pristine CNT allows it to render superior

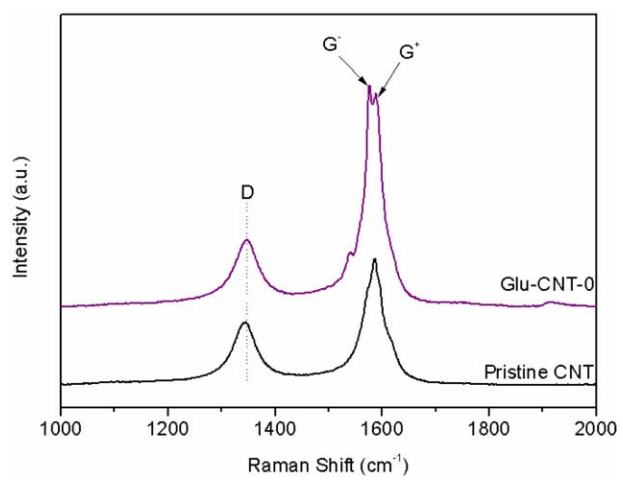

Figure 7. Raman spectra of Glu-CNT-0 and pristine CNT samples.

[Color figure can be viewed in the online issue, which is available at wileyonlinelibrary.com.]

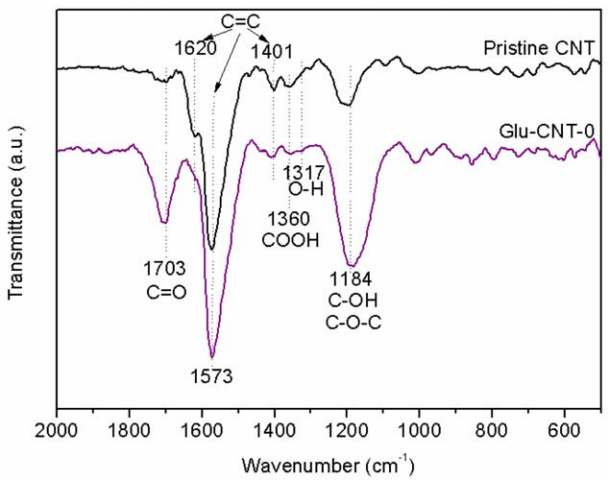

Figure 8. FTIR spectra of Glu-CNT-0 and pristine CNT samples.

[Color figure can be viewed in the online issue, which is available at wileyonlinelibrary.com.]

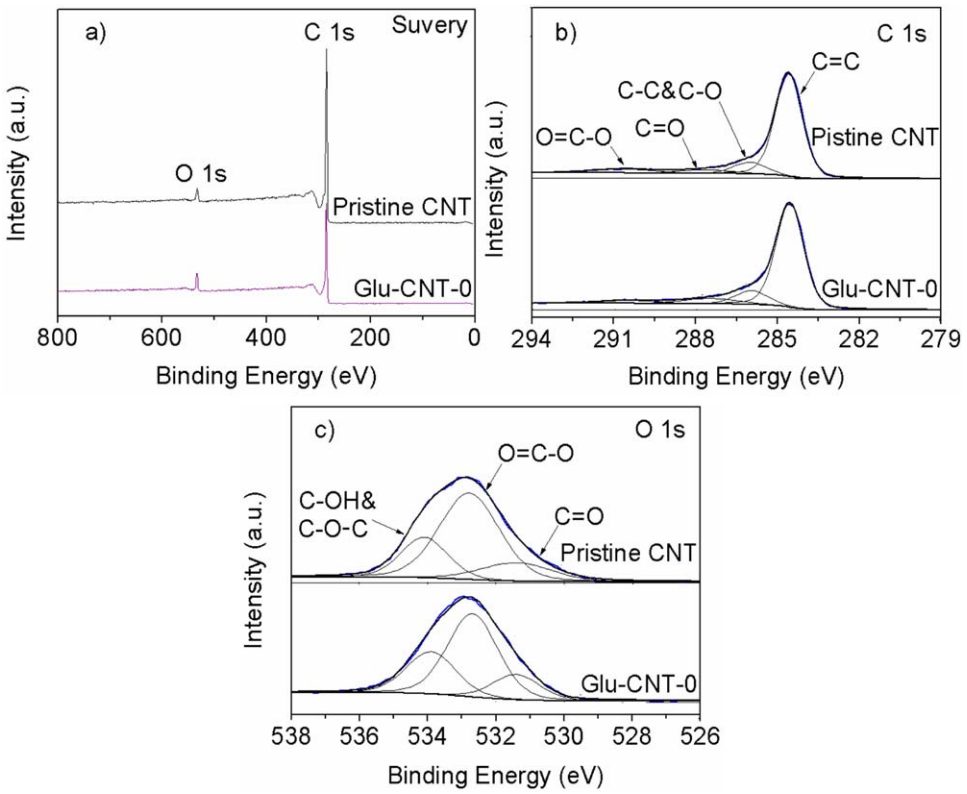

Figure 9. XPS spectra of Glu-CNT-0 and pristine CNT samples. (a) Suvery spectra, (b) C 1s, and (c) O 1s.

[Color figure can be viewed in the online issue, which is available at wileyonlinelibrary.com.]

activity, although it has lower surface C═O content. This could show that the surface structural defect sites may also active sites for C—H activation, which is consistent with the reported results in Ref. [46]. The developed M-Glu-CNT by GHT-PCM approach exhibits higher catalytic activity (4.6 mmol g^{-1} h^{-1} of steady-state rate) with similar selectivity to M-CNT (3.4 mmol g^{-1} h^{-1} of steady-state rate), which may be ascribed to the tuning in microstructure (increased surface structural defect, larger d-spacing, and absence of CNx in comparison with pristine CNT) and surface chemistry (increased surface C═O and N content) as identified by the HRTEM, BET, Raman, XRD, and XPS analytical results. The surface ketonic C═O and the structural defects are the active centers for the C—H activation, and high surface area and pore volume increase the accessibility of active sites to reactants, thus enhances the DDH. The developed M-Glu-CNT demonstrates 1.35 and 1.64 times the steady-state styrene rate of the M-CNT prepared without GHT process and the pristine CNT, respectively, which allows it to be a promising candidate for DDH reaction.

Effect of hydrothermal conditions

From above, it can be found that the GHT approach before pyrolysis for preparing N-doped CNT can efficiently tune the microstructure and surface chemistry. It can increase structural defects and d-spacing for graphene sheet as well as result in the increase in surface N and ketonic C═O group. As a result, the catalysis in DDH reaction can be efficiently enhanced. The effect of GHT conditions including glucose concentration, hydrothermal temperature, and hydrothermal time on the microstructure, surface chemistry, and the catalysis in DDH reaction is addressed below.

From HRTEM presented in Figure 11, the increase in glucose concentration can strengthen the structural defectiveness, but the 26.8% concentration is too high and leads to the existence of many carbon fragments on N-doped CNT

Table 2. Comparison of XPS Quantitative Analysis Results for Glu-CNT-0 with Those for Glu-CNT and Pristine CNT Samples

Sample	C-1[a] (%)	C-2[a] (%)	C-3[a] (%)	C-4[a] (%)	C-5[a] (%)	N[b] (%)	N-1[c] (%)	N-2[c] (%)	N-3[c] (%)	N-4[c] (%)	O[d] (%)	O-1[e] (%)	O-2[e] (%)	O-3[e] (%)
CNT	77.7	–	10.4	5.3	6.5	–	–	–	–	–	4.1	15.8	47.8	36.4
Glu-CNT-0	76.0	–	11.9	7.8	4.3	–	–	–	–	–	6.7	16.0	56.0	28.0

[a]Percentage of various nitrogen species occupying in the total C content; C-1, C-2, C-3, C-4, and C-5 are denoted as C═C, C—N, C—C/C—O, C═O/C═N, and O—C═O, respectively.
[b]The surface N content of the materials from XPS.
[c]Percentage of various nitrogen species occupying in the total N content; N-1, N-2, N-3, and N-4 are denoted as pyridinic N, pyrrolic N, graphitic N, and oxidized N, respectively.
[d]The O atom molar percentage on the material surface from XPS analysis.
[e]Percentage of various nitrogen species occupying in the total O content; O-1, O-2, and O-3 are denoted as C═O, O═C—O, and C—OH/C—O—C, respectively.

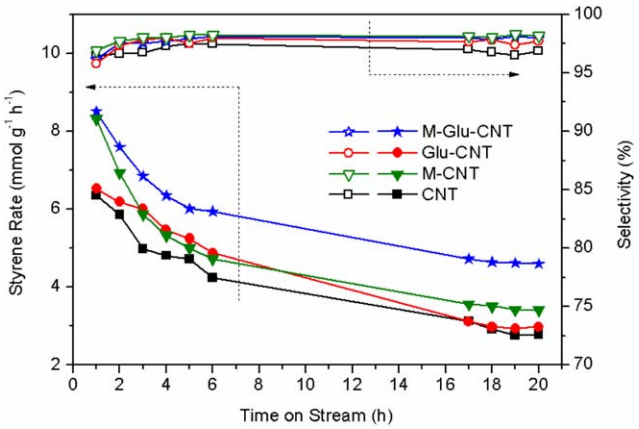

Figure 10. Catalytic performance of M-Glu-CNT, Glu-CNT, M-CNT, and the pristine CNT samples as a function of time on stream for direct dehydrogenation of ethylbenzene to styrene under oxidant- and steam-free conditions.

[Color figure can be viewed in the online issue, which is available at wileyonlinelibrary.com.]

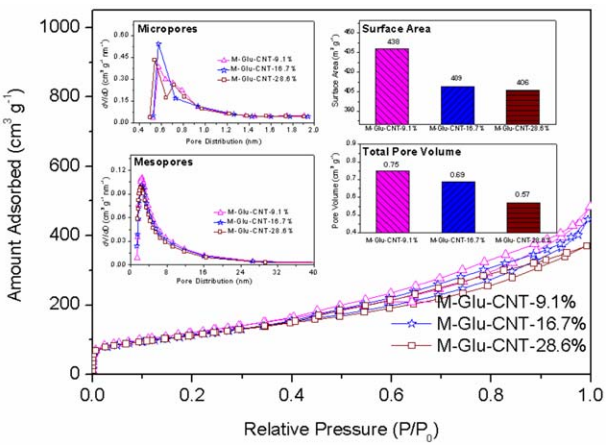

Figure 12. Nitrogen adsorption–desorption isotherms of the M-Glu-CNT-9.1%, M-Glu-CNT-16.7%, and M-Glu-CNT-28.6% samples. Insets: Barrett–Joyner–Halenda adsorption mesopore size distribution, Horvath–Kawazoe adsorption micropore size distribution, and specific surface area.

[Color figure can be viewed in the online issue, which is available at wileyonlinelibrary.com.]

sample. The wafted carbon fragments may inhibit the active sites from availability to reactants. As a result, the catalytic activity may be suppressed. As shown in Figure 12, the increase in the glucose concentration for the glucose hydrothermal process from 9.1 to 28.6% leads to the continuous decrease in surface area and pore volume but with similar pore distribution, suggesting the possible covering of the CNT surface by carbon fragment and/or the possible void-filling in the CNT by carbon fragments, which supports the observations by HRTEM.

From the XPS data in Figure 13 and Table 3, the increase in glucose concentration from 9.1 to 16.7% can increase surface N and O atom amount, ascribed to enhanced

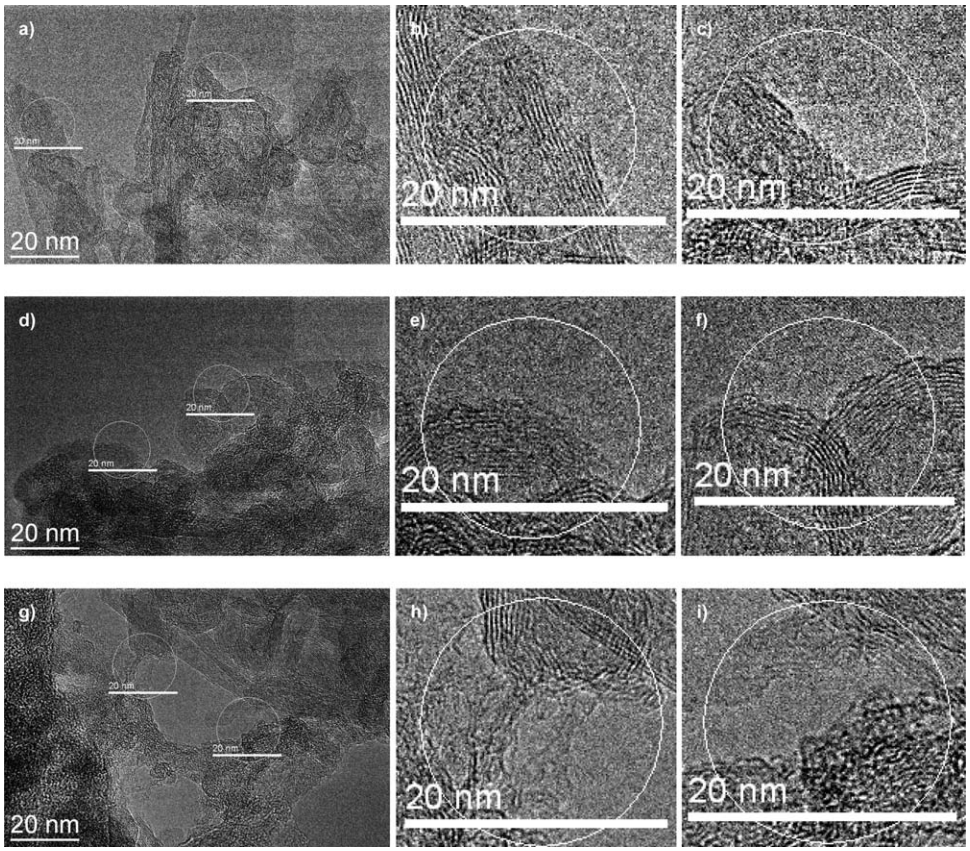

Figure 11. HRTEM images of (a–c) M-Glu-CNT-9.1%, (d–f) M-Glu-CNT-16.7%, and (g–i) M-Glu-CNT-28.6% samples.

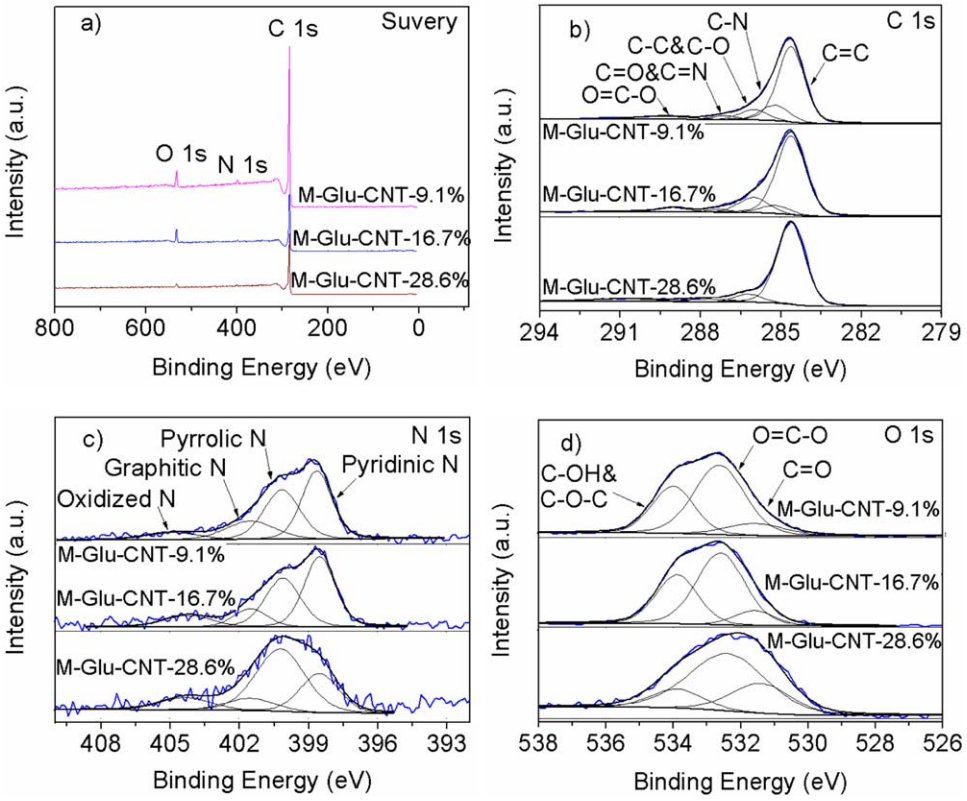

Figure 13. XPS spectra of M-Glu-CNT-9.1%, M-Glu-CNT-16.7%, and M-Glu-CNT-28.6% samples. (a) Suvery spectra and (b–d) C 1s, N 1s, and O 1s, respectively.

[Color figure can be viewed in the online issue, which is available at wileyonlinelibrary.com.]

defectiveness,[59] increased polysaccharide amount and intensified hydrogen bond of melamine with hydroxyl groups of polysaccharide. However, the further increase in glucose concentration leads to the decrease in surface N and O contents. This ascribed to the prohibition effect from floating carbon fragments (confirmed by HRTEM and BET measurement) on N and O incorporation into carbon matrix.

Figure 14 depicts the catalytic performance of the N-doped CNTs prepared by GHT-PCM approach with diverse glucose concentrations for DDH reaction of ethylbenzene. Results show that the increase in glucose concentration from 9.1 to 16.7% leads to the increase in steady-state rate from 3.9 to 4.6 mmol g^{-1} h^{-1}. However, the further increase in glucose concentration up to 28.6%, a decreasing activity (4.3 mmol g^{-1} h^{-1}) can be observed. The N-doped CNT prepared by GHT-PCM approach with optimum glucose concentration exhibits higher catalytic activity to the others, ascribed to more defect sites and larger amount of surface ketonic C═O group. The lower catalytic activity of M-Glu-CNT-28.6% in comparison with M-Glu-CNT-16.7% may be caused by the possible inhibition effect of floating carbon fragments blocking active sites from reactant. Also, there is a decrease in surface C═O, confirmed by HRTEM and BET experiments. Correlated the reaction results (reaction rate: 3.9, 4.6, and 4.3 mmol g^{-1} h^{-1}) to the XPS data (N percentage: 1.8, 1.9, and 1.6; C═O percentage: 0.48, 0.74, and 0.69), the Raman and HRTEM characterization results of the three samples M-Glu-CNT-9.1% M-Glu-CNT-16.7%, and M-Glu-CNT-28.6%, respectively, it can be concluded that the catalytic performance of modified CNT is strongly dependent on the microstructure and surface

Table 3. XPS Quantitative Analysis Results for M-Glu-CNT Samples Prepared with Diverse Glucose Mass Concentrations for the Controlled Hydrothermal Pretreatment of Pristine CNT for N-CNT Preparation Through a Facile Pyrolysis Approach in the Presence of Melamine

Sample	C-1[a] (%)	C-2[a] (%)	C-3[a] (%)	C-4[a] (%)	C-5[a] (%)	N[b] (%)	N-1[c] (%)	N-2[c] (%)	N-3[c] (%)	N-4[c] (%)	O[d] (%)	O-1[e] (%)	O-2[e] (%)	O-3[e] (%)
M-Glu-CNT-9.1%	65.6	14.8	9.4	3.4	5.8	1.8	40.1	34.9	17.6	7.4	4.2	11.5	56.5	32.0
M-Glu-CNT-16.7%	70.3	7.5	14.2	2.3	5.7	1.9	43.1	34.2	11.9	10.8	7.4	10.0	56.5	33.5
M-Glu-CNT-28.6%	74.7	5.8	7.1	5.6	6.9	1.6	26.0	52.6	10.4	11.0	2.8	24.9	61.1	14.0

[a]Percentage of various nitrogen species occupying in the total C content; C-1, C-2, C-3, C-4, and C-5 are denoted as C═C, C—N, C—C/C—O, C═O/C═N, and O—C═O, respectively.
[b]The surface N content of the materials from XPS.
[c]Percentage of various nitrogen species occupying in the total N content; N-1, N-2, N-3, and N-4 are denoted as pyridinic N, pyrrolic N, graphitic N, and oxidized N, respectively.
[d]The O atom molar percentage on the material surface from XPS analysis.
[e]Percentage of various nitrogen species occupying in the total O content; O-1, O-2, and O-3 are denoted as C═O, O═C—O, and C—OH/C—O—C, respectively.

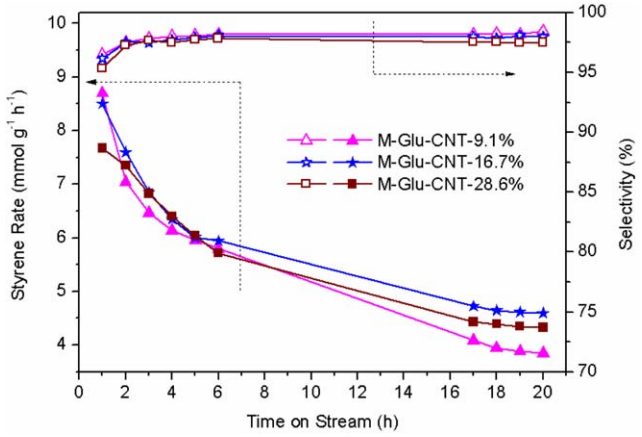

Figure 14. Catalytic performance of M-Glu-CNT-9.1%, M-Glu-CNT-16.7%, and M-Glu-CNT-28.6% samples as a function of time on stream for direct dehydrogenation of ethylbenzene to styrene under oxidant- and steam-free conditions.

[Color figure can be viewed in the online issue, which is available at wileyonlinelibrary.com.]

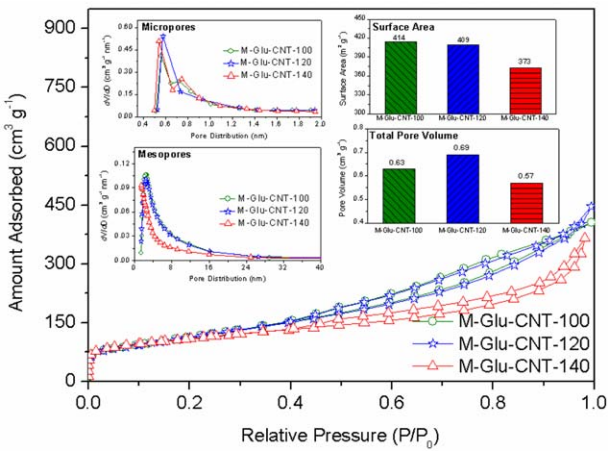

Figure 16. Nitrogen adsorption–desorption isotherms of the M-Glu-CNT-100, M-Glu-CNT-120, and M-Glu-CNT-140 samples. Insets: Barrett–Joyner–Halenda adsorption mesopore size distribution, Horvath–Kawazoe adsorption micropore size distribution, and specific surface area.

[Color figure can be viewed in the online issue, which is available at wileyonlinelibrary.com.]

properties. The surface C═O and structural defects are the main active sites for DDH with N-doping promoting the reactivity.

The glucose hydrothermal temperature may affect the polymerization degree (O content) of polysaccharide coating on CNT and also the amount of polysaccharide, which subsequently affects the microstructures and surface chemistry of as-synthesized N-doped CNTs by GHT-PCM approach. Therefore, the microstructures and surface chemistry of M-Glu-CNTs prepared by GHT-PCM method with diverse hydrothermal temperatures (100, 120, 140°C, and the optimized 16.7% glucose concentration was used for preparing

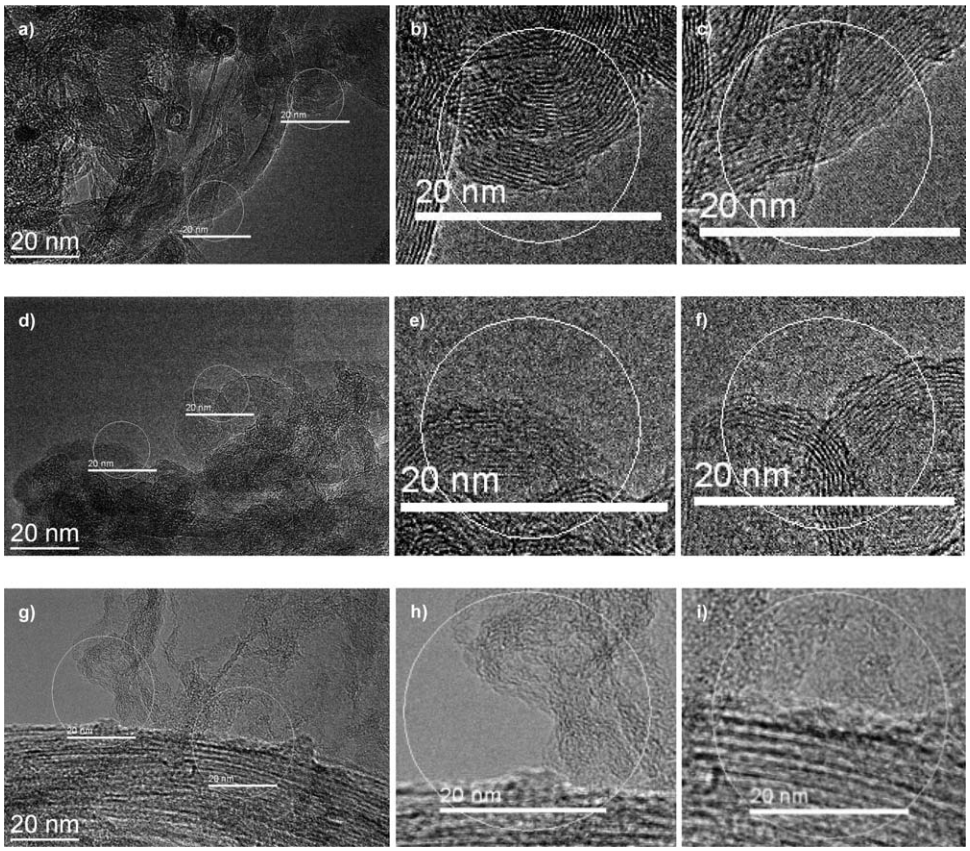

Figure 15. HRTEM images of (a–c) M-Glu-CNT-100, (d–f) M-Glu-CNT-120, and (g–i) M-Glu-CNT-140 samples.

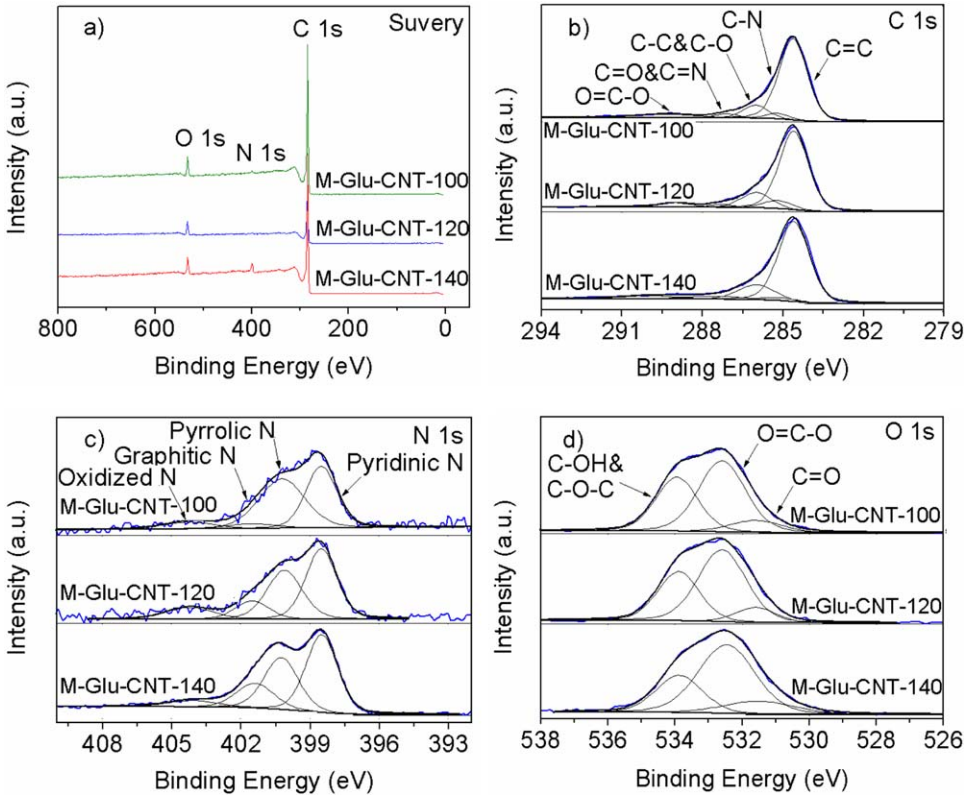

Figure 17. XPS spectra of M-Glu-CNT-100, M-Glu-CNT-120, and M-Glu-CNT-140 samples. (a) Suvery spectra and (b–d) C 1s, N 1s, and O 1s, respectively.

[Color figure can be viewed in the online issue, which is available at wileyonlinelibrary.com.]

M-Glu-CNT-100, 120, and 140) were investigated by HRTEM (Figure 15), BET (Figure 16), and XPS (Figure 17). The catalytic performance of each was evaluated using DDH as a model reaction (Figure 18).

From Figure 15, increased defectiveness can be seen as the hydrothermal temperature increases from 100 to 120°C, ascribed to more polysaccharide on CNT surface. However, no more defective sites but the clear floating carbon fragments on the M-Glu-CNT-140 surface can be seen. Interestingly, in comparison with M-Glu-CNT-28.6% prepared by GHT-PCM with higher glucose concentration, the M-Glu-CNT-140 prepared by GHT-PCM with 140°C of high hydrothermal temperature possesses visibly different morphology and surface features (Figures 11g–i and 15g–i). Besides the floating carbon fragment, we can also see carbon fragment layer coating on CNT surface, but it is different from the CNx on the M-CNT sample. Moreover, the higher hydrothermal temperature may result in increased polymerization of glucose for the formation of polysaccharide on CNT. The lower O content in polysaccharide may also lower surface O content on the as-synthesized N-doped CNT, which is unfavorable for DDH reaction. The change in the morphology and surface structure led by the different GHT temperature may affect the catalytic performance of N-doped CNT.

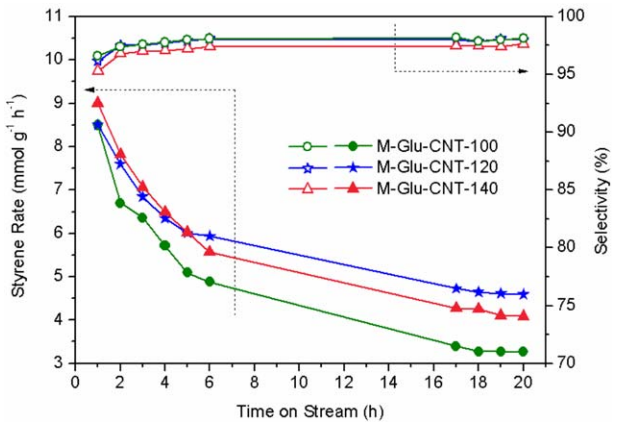

Figure 18. Catalytic performance of M-Glu-CNT-100, M-Glu-CNT-120, and M-Glu-CNT-140 samples as a function of time on stream for direct dehydrogenation of ethylbenzene to styrene under oxidant- and steam-free conditions.

[Color figure can be viewed in the online issue, which is available at wileyonlinelibrary.com.]

Figure 16 presents the nitrogen adsorption–desorption isotherms of the M-Glu-CNT-100, M-Glu-CNT-120, and M-Glu-CNT-140 samples. From Figure 16, the increasing hydrothermal temperature results in the decrease in surafce area, and especially the 373 $m^2\ g^{-1}$ of very low surface area for the M-Glu-CNT-140 can be observed. This is ascribed to the carbon fragment layer coating on CNT surface identified by HRTEM. Moreover, in comparison with the other two samples, the M-Glu-CNT-140 has smaller mesopore diameter. This is possibly caused by the carbon fragment from polysaccharide pyrolysis filling into the CNT. The BET results can efficiently support the observation on the samples by HRTEM.

Figure 17 presents the XPS spectra including survey, C1s, N1s, and O1s for the M-Glu-CNT-100, M-Glu-CNT-120,

Table 4. XPS Quantitative Analysis Results for M-Glu-CNT Samples Prepared with Diverse Glucose Hydrothermal Temperatures for the Controlled Hydrothermal Pretreatment of Pristine CNT for N-CNT Preparation Through a Facile Pyrolysis Approach in the Presence of Melamine

Sample	C-1[a] (%)	C-2[a] (%)	C-3[a] (%)	C-4[a] (%)	C-5[a] (%)	N[b] (%)	N-1[c] (%)	N-2[c] (%)	N-3[c] (%)	N-4[c] (%)	O[d] (%)	O-1[e] (%)	O-2[e] (%)	O-3[e] (%)
M-Glu-CNT-100	75.2	4.3	10.8	3.0	6.7	1.2	40.0	47.7	5.0	7.3	5.1	10.2	53.4	36.4
M-Glu-CNT-120	70.3	7.5	14.2	2.3	5.7	1.9	43.1	34.2	11.9	10.8	7.4	10.0	56.5	33.5
M-Glu-CNT-140	70.4	3.1	15.6	5.4	5.5	5.8	44.7	32.4	16.9	5.9	5.1	13.9	59.7	26.4

[a]Percentage of various nitrogen species occupying in the total C content; C-1, C-2, C-3, C-4, and C-5 are denoted as C═C, C─N, C─C/C─O, C═O/C═N, and O─C═O, respectively.
[b]The surface N content of the materials from XPS.
[c]Percentage of various nitrogen species occupying in the total N content; N-1, N-2, N-3, and N-4 are denoted as pyridinic N, pyrrolic N, graphitic N, and oxidized N, respectively.
[d]The O atom molar percentage on the material surface from XPS analysis.
[e]Percentage of various nitrogen species occupying in the total O content; O-1, O-2, and O-3 are denoted as C═O, O═C─O, and C─OH/C─O─C, respectively.

and M-Glu-CNT-140. Table 4 gives the quantitative XPS results. From Figure 17a and Table 4, we can see the continuously increased N content as the hydrothermal temperature rises from 100 to 140°C, which is due to the promoting effect of hydrogen bond between the formed polysaccharide and melamine on N-doping. Interestingly, the M-Glu-CNT-140 (Figures 17a, c and Table 4) has higher N content in comparison of M-Glu-CNT-28.6% (Figure 13 and Table 3) although both of them have floating carbon fragments. From Figures 15g–i, besides the floating carbon fragment, we can see the carbon fragment layer coating on CNT (also confirmed by BET measurement), which is favorable for the N-doping by the forming hydrogen bonds. Furthermore, although the explosive decomposition of polysaccharide, the N-content on M-Glu-CNT-140 is even higher than that on M-CNT, which further confirms the promoting effect of GHT process on N-doping. As a result, the surface N content may be increased on the as-prepared M-Glu-CNT-140 by the GHT process with a higher temperature. From 14b, the C1s spectra of the three samples can be deconvoluted into five speaks corresponding to C═C, C─N, C─C/C─O, C═O/C═N, O─C═O, linked with the N 1s spectra, the N atom incorporation into carbon matrix can be clearly confirmed. Furthermore, From Figure 17d and Table 4, with the increase in hydrothermal temperature from 100 to 120°C, surface O atom content is increased from 5.1 to 7.4 At %, resulted from higher O atoms from more polysaccharide levels formed by GHT process at higher temperature. However, the further increase in hydrothermal temperature up to 140°C may lead to higher polymerization degree, which lowers the O concentration in polysaccharide. As a result, the lower O content on M-Glu-CNT-140 can be observed.

From Figure 18, as the hydrothermal temperature is increased from 100 to 120°C, the steady-state styrene rate increases from 3.3 to 4.6 mmol g^{-1} h^{-1}. Correlated to the characterization results by HRTEM and XPS, the higher catalytic activity may be ascribed to the heightened surface structural defectiveness and richer surface C═O. However, the decrease in styrene rate on M-Glu-CNT-140 in comparison with M-Glu-CNT-120 can be observed, which might be ascribed to the lowering C═O content and the inhibiting effect of floating carbon fragment confirmed by HRTEM and BET measurement on the active sites accessibility. Moreover, although M-Glu-CNT-140 has 5.8 At % of highest N content, it exhibits medium activity, suggesting that N-doping can enhance the catalytic performance of CNT, but it cannot have decisive effect on catalytic performance. From Refs. 39 and 51, the surface ketonic C═O group and structural defects are active species for C─H activation. The catalytic activity is also strongly dependent on accessibility of active species. The M-Glu-CNT-120 possesses increased structural defects and enriched ketonic C═O, but no floating carbon fragment or carbon fragment layers on its surface. Therefore, it demonstrates much better catalytic activity with similar selectivity than the other two samples.

Moreover, hydrothermal time is another factor influencing the formed polysaccharide. However, it mainly affects the amount of polysaccharide, but not the polymerization degree. This differs from the effect of hydrothermal temperature. Therefore, the effect of hydrothermal time on the microstructure, surface chemistry, and the catalytic performance in DDH reaction was investigated. Figure 19 presents the HRTEM images of the N-doped CNTs prepared by the developed GHT-PCM approach in this work using optimized 16.7% glucose concentration but with diverse hydrothermal times (M-Glu-CNT-10, M-Glu-CNT-20, and M-Glu-CNT-40). From Figure 19, no floating carbon fragment can be observed on the M-Glu-CNT-10, M-Glu-CNT-20, and even on M-Glu-CNT-40. The longer hydrothermal time can lead to more polysaccharide formed on CNT, but not polymerization degree, and therefore, more O atoms exist in polysaccharide. This is different from the effect of hydrothermal temperature. As a result, there is different change in microstructure of N-doped CNTs, although the increase in either hydrothermal time or temperature can enlarge the amount of polysaccharide. Although the surface structural defects formed by explosive decomposition of polysaccharide can be strengthened by prolonging hydrothermal time, too long of a hydrothermal time may lead to the formation of carbon fragments on N-doped CNT (M-Glu-CNT-40, Figures 19g–i). The HRTEM observation can be further identified by the BET analysis shown in Figure 20. Although the hydrothermal time does not affect the pore distribution, the continuous decrease in both surface area and pore volume can be observed along with the extension of the hydrothermal time from 10 to 40 h. This suggests possible covering of carbon fragment on the surface or filling into the CNT. Shorter hydrothermal times cannot produce enough polysaccharide for structural defect production and surface O enrichment; however, longer hydrothermal times lead to the formation of many carbon fragments, which may decrease the accessibility of active sites to reactants by the inhibition effect of floating carbon fragment or the carbon covering on the CNT.

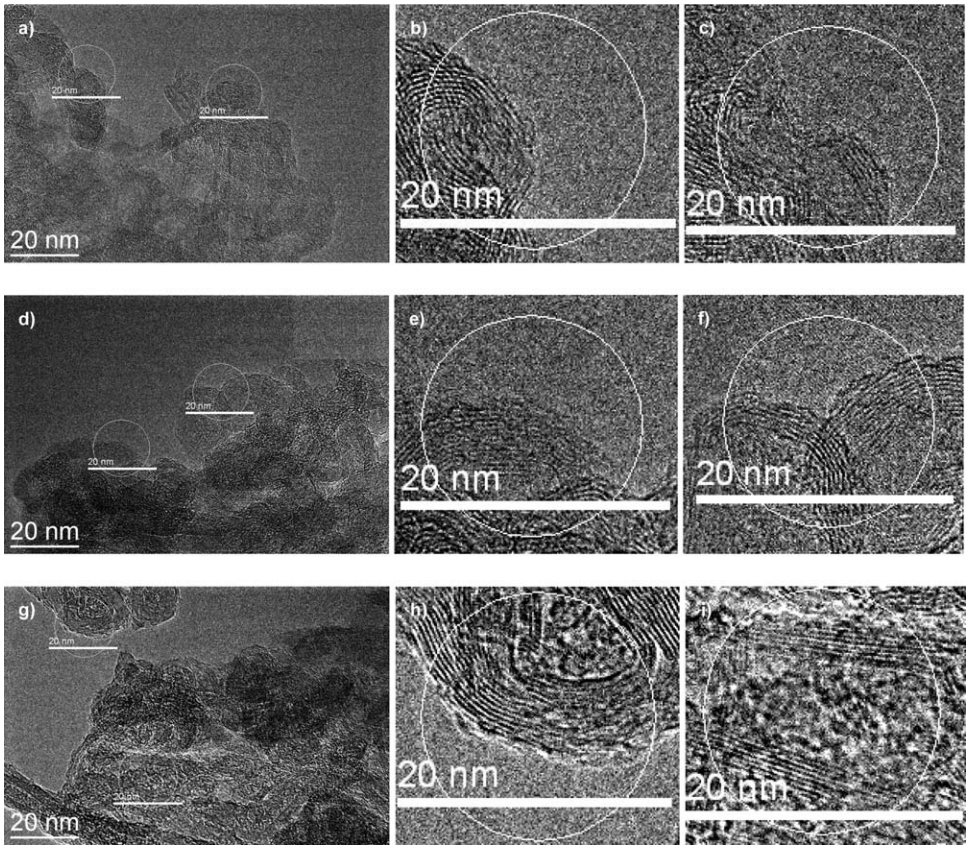

Figure 19. HRTEM images of (a–c) M-Glu-CNT-10, (d–f) M-Glu-CNT-20, and (g–i) M-Glu-CNT-40 samples.

In Figure 21 and Table 5, the higher polysaccharide amounts from increasing hydrothermal time from 10 to 40 h can continuously increase both N and O contents of the N-doped CNTs. However, like the effect of glucose concentration, only slight changes can be observed. No significant increase in N content can be observed even if the hydrothermal time is increased from 10 to 40 h. Interestingly, from Figure 21a and Table 5, we observe that the O content on N-doped CNTs continuously rise from 1.4 to 9.8 At % as the hydrothermal time increases from 10 to 40 h. However, with the increase in glucose concentration or hydrothermal temperature, the O atom content on N-doped CNTs first increases and reaches the maximum, and then decreases. The data show that the increased polysaccharide is achieved by increasing glucose concentration, raising hydrothermal temperature, or prolonging hydrothermal time in order to increase the O content on the surface of N-doped CNTs. However, the decreased O content on both M-Glu-CNT-28.6% and M-Glu-CNT-140 can be observed (Table 3 and Supporting Information Table S4). Correlated the XPS data for M-Glu-CNT-28.6%, M-Glu-CNT-140, and N-Glu-CNT-40 to the HRTEM images, it can be proposed that increase in glucose concentration, hydrothermal temperature, and hydrothermal time has different influence on the component and structure of the polysaccharide, although all of them can increase the amount of polysaccharide. As a result, the microstructure and surface chemical properties of N-doped CNTs can be efficiently tailored, which subsequently affects their catalytic performance. Although M-Glu-CNT-40 has highest surface O atom content, the lower C=O content on its surface is observed (Figure 21d and Table 5), which may lead to lower catalytic performance in DDH reaction.

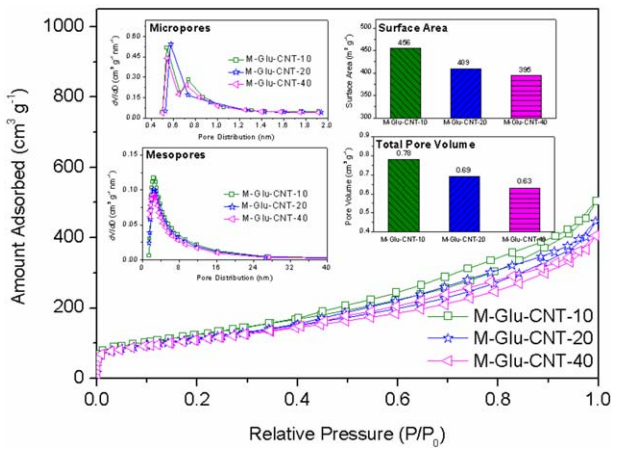

Figure 20. Nitrogen adsorption–desorption isotherms of the M-Glu-CNT-10, M-Glu-CNT-20, and M-Glu-CNT-40 samples. Insets: Barrett–Joyner–Halenda adsorption mesopore size distribution, Horvath–Kawazoe adsorption micropore size distribution, and specific surface area.

[Color figure can be viewed in the online issue, which is available at wileyonlinelibrary.com.]

From Figure 22, the steady-state styrene rate rises from 3.7 to 4.6 mmol g^{-1} h^{-1} as the hydrothermal time is increased from 10 to 20 h, ascribed to the more surface

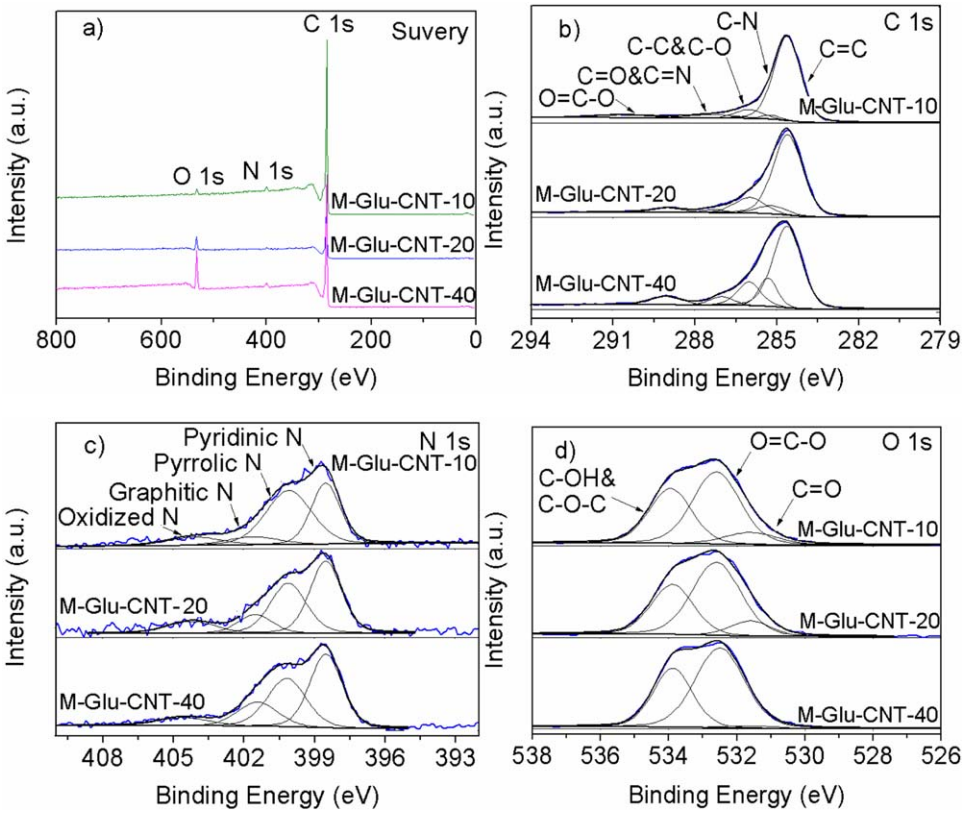

Figure 21. XPS spectra of M-Glu-CNT-10, M-Glu-CNT-20, and M-Glu-CNT-40 samples. (a) Suvery spectra and (b–d) C 1s, N 1s, and O 1s, respectively.

[Color figure can be viewed in the online issue, which is available at wileyonlinelibrary.com.]

defects and higher C═O content. The decrease in reaction rate can be obtained as the hydrothermal time is further prolonged from 20 to 40 h, ascribed to lower surface C═O amount (Table 5) and also lower accessibility of active sites to reactants inhibited by obstructing carbon fragment (Figures 19g–i). The M-Glu-CNT-40 exhibits higher catalytic activity than M-Glu-CNT-10, although the former has lower amount of surface ketonic C═O than the latter, possibly ascribed to the intensified promoting effect by increased N content. From above, the microstructure and surface chemistry of N-doped CNTs can be efficiently tuned by the introduction of glucose hydrothermal pretreatment before pyrolysis and the conditions for the GHT process. As a results, the amount and the accessibility of active sites especially surface ketonic C═O group/structural defects can be subsequently modulated. The as-prepared N-doped CNTs by the developed GHT-PCM approach exhibits higher catalytic performance to the M-CNT prepared by pyrolysis of pristine CNT with melamine but without GHT process.

Extending GHT-PCM approach to other carbocatalysts

To investigate whether the developed GHT-PCM approach can be extended to the farbication of the other N-doped carbonaceous materials with enhanced catalysis, a comparison of the catalytic performance of the M-Glu-CMK-3 with M-CMK-3 and CMK-3 for DDH reaction was made. The reaction results are illustrated in Figure 23. The results show that the M-Glu-CMK-3 catalyst prepared by the developed GHT-PCM method demonstrates higher catalytic performance to the M-CMK-3 catalyst prepared by traditional pyrolysis method by heating the mixture of mesoporous carbon and melamine. The results illustrate that the directed GHT-PCM

Table 5. XPS Quantitative Analysis Results for M-Glu-CNT Samples Prepared with Diverse Glucose Hydrothermal Times for the Controlled Hydrothermal Pretreatment of Pristine CNT for N-CNT Preparation Through a Facile Pyrolysis Approach in the Presence of Melamine

Sample	C-1[a] (%)	C-2[a] (%)	C-3[a] (%)	C-4[a] (%)	C-5[a] (%)	N[b] (%)	N-1[c] (%)	N-2[c] (%)	N-3[c] (%)	N-4[c] (%)	O[d] (%)	O-1[e] (%)	O-2[e] (%)	O-3[e] (%)
M-Glu-CNT-10	77.1	2.6	8.4	6.0	5.9	1.9	21.6	30.5	42.5	5.5	1.4	38.4	47.1	14.5
M-Glu-CNT-20	70.3	7.5	14.2	2.3	5.7	1.9	43.1	34.2	11.9	10.8	7.4	10.0	56.5	33.5
M-Glu-CNT-40	60.0	13.4	14.5	5.3	6.8	2.4	42.0	33.3	17.1	7.6	9.8	2.5	61.5	36.0

[a]Percentage of various nitrogen species occupying in the total C content; C-1, C-2, C-3, C-4, and C-5 are denoted as C═C, C—N, C—C/C—O, C═O/C═N, and O—C═O, respectively.
[b]The surface N content of the materials from XPS.
[c]Percentage of various nitrogen species occupying in the total N content; N-1, N-2, N-3, and N-4 are denoted as pyridinic N, pyrrolic N, graphitic N, and oxidized N, respectively.
[d]The O atom molar percentage on the material surface from XPS analysis.
[e]Percentage of various nitrogen species occupying in the total O content; O-1, O-2, and O-3 are denoted as C═O, O═C—O, and C—OH/C—O—C, respectively.

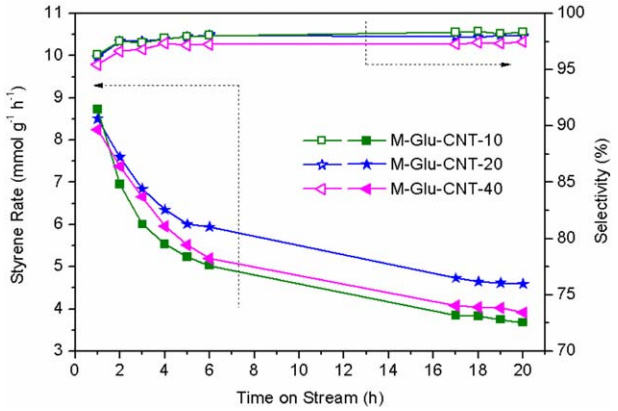

Figure 22. Catalytic performance of M-Glu-CNT-10, M-Glu-CNT-20, and M-Glu-CNT-40 samples as a function of time on stream for direct dehydrogenation of ethylbenzene to styrene under oxidant- and steam-free conditions.

[Color figure can be viewed in the online issue, which is available at wileyonlinelibrary.com.]

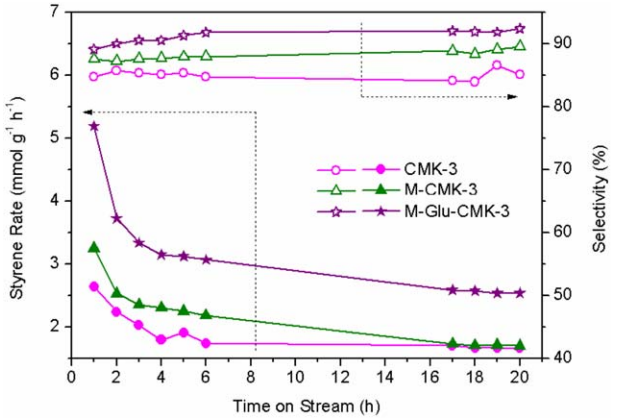

Figure 23. Catalytic performance of M-Glu-CMK-3, M-CMK-3, and CMK-3 samples as a function of time on stream for direct dehydrogenation of ethylbenzene to styrene under oxidant- and steam-free conditions.

[Color figure can be viewed in the online issue, which is available at wileyonlinelibrary.com.]

approach developed in this work may be extended to prepare diverse N-doped carbonaceous materials with promoted catalytic performance. These novel and efficient materials and techniques can be used for the DDH reaction for styrene production and possibly in other such reactions.

Conclusions

In summary, we present a facile and scalable prior controlled GHT and subsequently pyrolysis approach for fabricating N-doped carbonaceous materials with controllable microstructure and surface chemical properties. The characterization results demonstrate that the prior GHT and its conditions including glucose concentration, hydrothermal temperature, and hydrothermal time significantly affect material microstructure and surface chemical properties of the as-prepared N-doped carbonaceous materials, which subsequently influences the catalytic performance in DDH reaction for styrene production. The optimized M-Glu-CNT catalyst demonstrates 1.35 and 1.64 times the steady-state styrene rate of the M-CNT prepared without GHT treatment and the pristine CNT, respectively, which endows it with great potential for future clean production of styrene over metal-free carbocatalyst under oxidant- and steam-free conditions. The surface kenotic C═O and structural defect are active sites for the DDH reaction; the improved nucleophilicity of C═O and basic properties of materials caused by N-doping can efficiently intensify the performance of active sites.[43–48] The superior catalytic performance of the developed M-Glu-CNT catalyst in this work can be ascribed to increased structural defects, enriched surface ketonic C═O group, and the promoted N-doping on the M-Glu-CNT by surface hydroxyl groups from GHT. Furthermore, the hydorthermal conditions can significantly change the microstructure and surface chemistry of the modified CNT catalysts. Insufficient hydorthermal conditions cannot produce enough polysaccharide formation for increasing structural defects and removing the heavy CNx from melamine and enriching suraface oxygen. However, overly severe hydorthermal conditions can lead to carbon fragments from polysaccharide decomposition. The produced structural defects and surface C═O can activate the C—H bonds and catalyze the DDH reaction of ethylbenzene. However, the residual carbon fragments can depress the accessibility of acive sites to reactants to decrease the catalytic activity. The appropriate hydorthermal conditions are essential to fabricate the C═O and defect-rich N-doped CNT catalysts. The established prior controlled GHT and subsequently pyrolysis approach can be extended to the fabrication of the other N-doped carbonaceous materials. Results show that the novel N-doped mesoporous carbon (M-Glu-CMK-3) by the directed approach indicates 1.47 times the styrene rate of the common N-doped CMK-3 (M-CMK-3, without glucose hydrothermal pretreatment). Therefore, we can safely say that the developed prior controlled GHT and subsequently pyrolysis strategy in this work would be considered as a facile and efficient strategy for fabricating diverse N-doped carbonaceous catalysts with excellent catalytic performance in DDH reaction with possibly extension to the other metal-free carbocatalytic reactions.

Acknowledgment

This work is financially supported by the National Natural Science Foundation of China (Grant nos. 20803006 and 21276041), the Joint Fund of Coal, set up by National Natural Science Foundation of China and Shenhua Co., Ltd. (no. U1261104), and also sponsored by the Chinese Ministry of Education via the Program for New Century Excellent Talents in University (Grant no. NCET-12-0079) and by the Fundamental Research Funds for the Central Universities (DUT15LK41).

Literature Cited

1. Su C, Loh KP. Carbocatalysts: graphene oxide and its derivatives. *Acc Chem Res*. 2013;46:2275–2285.
2. Sun X, Wang R, Su DS. Research progress in metal-free carbon-based catalysts. *Chin J Catal*. 2013;34:508–523.
3. Schaetz A, Zeltner M, Stark WJ. Carbon modifications and surfaces for catalytic organic transformations. *ACS Catal*. 2012;2:1267–1284.
4. Zhang J, Liu X, Blume R, Zhang AH, Schlöl R, Su DS. Surface-modified carbon nanotubes catalyze oxidative dehydrogenation of *n*-butane. *Science*. 2008;322:73–77.

5. Bedia J, Ruiz-Rosas R, Rodríguez-Mirasol J, Cordero T. Kinetic study of the decomposition of 2-butanol on carbon-based acid catalyst. *AIChE J*. 2010;56:1557–1568.
6. Ji P, Tan H, Xu X, Feng W. Lipase covalently attached to multiwalled carbon nanotubes as an efficient catalyst in organic solvent. *AIChE J*. 2010;56:3005–3011.
7. Younessi-Sinaki M, Hamdullahpur F. Numerical investigation on the number of active surface sites of carbon catalysts in the decomposition of methane. *AIChE J*. 2014;60:2228–2234.
8. Degirmenci L, Oktar N, Dogu G. Activated carbon supported silicotungstic acid catalysts for ethyl-tert-butyl ether synthesis. *AIChE J*. 2011;57:3171–3181.
9. Kong XK, Chen CL, Chen QW. Doped graphene for metal-free catalysis. *Chem Soc Rev*. 2014;43:2841–2857.
10. Ito Y, Qiu HJ, Fujita T, Tanabe Y, Tanigaki K, Chen M. Bicontinuous nanoporous N-doped graphene for the oxygen reduction reaction. *Adv Mater*. 2014;26:4145–4150.
11. Gong K, Du F, Xia Z, Durstock M, Dai L. Nitrogen-doped carbon nanotube arrays with high electrocatalytic activity for oxygen reduction. *Science*. 2009;323:760–764.
12. Li XH, Antonietti M. Metal nanoparticles at mesoporous N-doped carbons and carbon nitrides: functional Mott-Schottky heterojunctions for catalysis. *Chem Soc Rev*. 2013;42:6593–6604.
13. Wang H, Maiyalagan T, Wang X. Review on recent progress in nitrogen-doped graphene: synthesis, characterization, and its potential applications. *ACS Catal*. 2012;2:781–794.
14. Zhang S, Kang P, Ubnoske S, Brennaman MK, Song N, House RL, Glass JT, Meyer TJ. Polyethylenimine-enhanced electrocatalytic reduction of CO_2 to formate at nitrogen-doped carbon nanomaterials. *J Am Chem Soc*. 2014;136:7845–7848.
15. Park M, Ryu J, Kim Y, Cho J. Corn protein-derived nitrogen-doped carbon materials with oxygen-rich functional groups: a highly efficient electrocatalyst for all-vanadium redox flow batteries. *Energy Environ Sci*. 2014;7:3727–3735.
16. Velasco LF, Lima JC, Ania C. Visible-light photochemical activity of nanoporous carbons under monochromatic light. *Angew Chem Int Ed*. 2014;53:4146–4148.
17. Sgobba V, Guldi, DM. Carbon nanotubes-electronic/electrochemical properties and application for nanoelectronics and photonics. *Chem Soc Rev*. 2009;38:165–184.
18. Gao S, Chen Y, Fan H, Wei X, Hu C, Wang L, Qu L. A green one-arrow-two-hawks strategy for nitrogen-doped carbon dots as fluorescent ink and oxygen reduction electrocatalysts. *J Mater Chem A*. 2014;2:6320–6325.
19. Tang L, Ji R, Li X, Bai G, Liu CP, Hao J, Lin J, Jiang H, Teng KS, Yang Z, Lau SP. Deep ultraviolet to near-infrared emission and photoresponse in layered N-doped graphene quantum dots. *ACS Nano*. 2014;8:6312–6320.
20. Lee JM, Park JS, Lee SH, Kim H, Yoo S, Kim SO. Selective electron- or hole-transport enhancement in bulk-heterojunction organic solar cells with N- or B-doped carbon nanotubes. *Adv Mater*. 2011; 23:629–633.
21. Lu L, Xu T, Chen W, Lee JM, Luo Z, Jung IH, Park HI, Kim SO, Yu L. The role of N-doped multiwall carbon nanotubes in achieving highly efficient polymer bulk heterojunction solar cells. *Nano Lett*. 2013;13:2365–2369.
22. Wu ZL, Gao MX, Wang TT, Wan XY, Zheng LL, Huang CZ. A general quantitative pH sensor developed with dicyandiamide N-doped high quantum yield graphene quantum dots. *Nanoscale*. 2014; 6:3868–3874.
23. Shalini J, Sankaran KJ, Dong CL, Lee CY, Tai NH, Lin IN. In situ detection of dopamine using nitrogen incorporated diamond nanowire electrode. *Nanoscale*. 2013;5:1159–1167.
24. Chen Y, Li X, Park K., Song J, Hong J, Zhou L, Mai YW, Huang H, Goodenough JB. Hollow carbon-nanotube/carbon-nanofiber hybrid anodes for Li-ion batteries. *J Am Chem Soc*. 2013;135: 16280–16283.
25. Song H, Li N, Cui H, Wang C. Enhanced storage capability and kinetic processes by pores- and hetero-atoms-riched carbon nanobubbles for lithium-ion and sodium-ion batteries anodes. *Nano Energy*. 2014;4:81–87.
26. Qie L, Chen WM, Wang ZH, Shao QG, Li X, Yuan LX, Hu XL, Zhang WX, Huang YH. Nitrogen-doped porous carbon nanofiber webs as anodes for lithium ion batteries with a superhigh capacity and rate capability. *Adv Mater*. 2012;24:2047–2050.
27. Long C, Qi D, Wei T, Yan J, Jiang L, Fan Z. Nitrogen-doped carbon networks for high energy density supercapacitors derived from polyaniline coated bacterial cellulose. *Adv Funct Mater*. 2014;24:3953–3961.
28. Feng S, Li W, Shi Q, Li Y, Chen J, Ling Y, Asirib AM, Zhao D. Synthesis of nitrogen-doped hollow carbon nanospheres for CO_2 capture. *Chem Commun*. 2014;50:329–331.
29. Zhuang X, Zhang F, Wu D, Feng X. Graphene coupled Schiff-base porous polymers: towards nitrogen-enriched porous carbon nanosheets with ultrahigh electrochemical capacity. *Adv Mater*. 2014;26: 3081–3086.
30. Wood KN, O'Hayre R, Pylypenko S. Recent progress on nitrogen/carbon structures designed for use in energy and sustainability applications. *Energy Environ Sci*. 2014;7:1212–1249.
31. Lee WJ, Maiti UN, Lee JM, Lim J, Han TH, Kim SO. Nitrogen-doped carbon nanotubes and graphene composite structures for energy and catalytic applications. *Chem Commun*. 2014;50:6818–6830.
32. Sheng ZH, Shao L, Chen JJ, Bao WJ, Wang FB, Xia XH. Catalyst-free synthesis of nitrogen-doped graphene via thermal annealing graphite oxide with melamine and its excellent electrocatalysis. *ACS Nano*. 2011;5:4350–4358.
33. Jin J, Fu X, Liu Q, Liu Y, Wei Z, Niu K, Zhang JL. Identifying the active site in nitrogen-doped graphene for the VO^{2+}/VO^{2+} redox reaction. *ACS Nano*. 2013;7:4764–4773.
34. Lin Z, Waller G, Liu Y, Liu M, Wong CP. Facile synthesis of nitrogen-doped graphene via pyrolysis of graphene oxide and urea, and its electrocatalytic activity toward the oxygen-reduction reaction. *Adv Energy Mater*. 2012;2:884–888.
35. Xue Y, Wu B, Jiang L, Guo Y, Huang L, Chen J, Tan J, Geng D, Luo B, Hu W, Yu G, Liu Y. Low temperature growth of highly nitrogen-doped single crystal graphene arrays by chemical vapor deposition. *J Am Chem Soc*. 2012;134:11060–11063.
36. Su C, Acik M, Takai K, Lu J, Hao S, Zheng Y, Wu P, Bao Q, Enoki T, Chabal YJ, Loh KP. Probing the catalytic activity of porous graphene oxide and the origin of this behaviour. *Nat Commun*. 2012;3:1298.
37. Gao Y, Ma D, Wang C, Guan J, Bao X. Reduced graphene oxide as a catalyst for hydrogenation of nitrobenzene at room temperature. *Chem Commun*. 2011;47:2432–2434.
38. Zhu J, Holmen A, Chen D. Carbon nanomaterials in catalysis: proton affinity, chemical and electronic properties, and their catalytic consequences. *ChemCatChem*. 2013;5:378–401.
39. Zhao ZK, Dai YT. Nanodiamond/carbon nitride hybrid nanoarchitecture as an efficient metal-free catalyst for oxidant- and steam-free dehydrogenation. *J Mater Chem A*. 2014;2:13442–13451.
40. Shekhah O, Ranke W, Schle A, Kolios G, Schlögl R. Styrene synthesis: high conversion over unpromoted iron oxide catalysts under practical working conditions. *Angew Chem Int Ed*. 2003;42:5760–5763.
41. Cavani F, Trifiro F. Alternative processes for the production of styrene. *Appl Catal A: Gen*. 1995;133:219–239.
42. Addiego WP, Estrada CA, Goodman DW, Rosynek MP. An infrared study of the dehydrogenation of ethylbenzene to styrene over iron-based catalysts. *J Catal*. 1994;146:407–414.
43. Zhang J, Su DS, Blume R, Schlögl R, Wang R, Yang X, Gajović A. Surface chemistry and catalytic reactivity of a nanodiamond in the steam-free dehydrogenation of ethylbenzene. *Angew Chem Int Ed*. 2010;49:8640–8644.
44. Zhao ZK, Dai YT, Lin JH, Wang GR. Highly-ordered mesoporous carbon nitride with ultrahigh surface area and pore volume as a superior dehydrogenation catalyst. *Chem Mater*. 2014;26:3151–3161.
45. Zhao ZK, Dai YT, Ge GF. Nitrogen-doped nanotubes-decorated activated carbon-based hybrid nanoarchitecture as superior catalyst for direct dehydrogenation. *Catal Sci Technol*. 2015;5:1548–1557.
46. Wang R, Sun X, Zhang B, Sun X, Su D. Hybrid nanocarbon as a catalyst for direct dehydrogenation of propane: formation of an active and selective core-shell sp^2/sp^3 nanocomposite structure. *Chem Eur J*. 2014;20:6324–6331.
47. Zhao ZK, Dai YT, Ge GF, Mao Q, Rong ZM, Wang GR. a facile approach to fabricate N-doped mesoporous graphene/nanodiamond hybrid nanocomposite with synergistically enhanced catalysis. *ChemCatChem*. 2015;7:1070–1077.
48. Zhao ZK, Dai YT, Ge GF, Wang GR. Guanidine nitrate enhanced catalysis of nitrogen-doped carbon nanotube for metal-free styrene production via direct dehydrogenation. *ChemCatChem*. 2015;7:1135–1144.
49. Zhao D, Huo Q, Feng J, Chmelka BF, Stucky GD. Nonionic triblock and star diblock copolymer and oligomeric surfactant syntheses of

highly ordered, hydrothermally stable, mesoporous silica structures. *J Am Chem Soc*. 1998;120:6024–6036.
50. Zhao D, Feng J, Huo Q, Melosh N, Fredrickson GH, Chmelka BF, Stucky GD. Triblock copolymer syntheses of mesoporous silica with periodic 50 to 300 angstrom pores. *Science*. 1998;279:548–552.
51. Jun S, Joo SH, Ryoo R, Kruk M, Jaroniec M, Liu Z, Ohsuna T, Terasaki O. Incorporation of N_2 and CO into organic molecules: amide formation by palladium-catalyzed carbonylation and nitrogenation. *J Am Chem Soc*. 2000;122:10712–10713.
52. Shao D, Tang D, Maia Y, Zhang L. Nanostructured silicon/porous carbon spherical composite as a high capacity anode for Li-ion batteries. *J Mater Chem A*. 2013;1:15068–15075.
53. Zheng X, Lv W, Tao Y, Shao J, Zhang C, Liu D, Luo J, Wang DW, Yang QH. Oriented and interlinked porous carbon nanosheets with an extraordinary capacitive performance. *Chem Mater*. 2014;26: 6896–6903.
54. Wu P, Qian Y, Du P, Zhang H, Cai C. Facile synthesis of nitrogen-doped graphene for measuring the releasing process of hydrogen peroxide from living cells. *J Mater Chem*. 2012;22:6402–6412.
55. Muramatsu H, Fujisawa K, ImKo Y, Yang KS, Hayashi T, Endo M, Yang CM, Jung YC, Kim YA. A selective way to create defects by the thermal treatment of fluorinated double walled carbon nanotubes. *Chin J Catal*. 2014;35:864–868.
56. Han C, Doepke A, Cho W, Likodimos V, de la Cruz AA., Back T, Heineman WR, Halsall HB, Shanov VN, Schulz MJ, Falaras P, Dionysiou DD. A multiwalled-carbon-nanotube-based biosensor for monitoring microcystin-LR in sources of drinking water supplies. *Adv Funct Mater*. 2013;23:1807–1816.
57. Ji CC, Xu MW, Bao SJ, Cai CJ, Lu ZJ, Chai H, Yang F, Wei H. Self-assembly of three-dimensional interconnected graphene-based aerogels and its application in supercapacitors. *J Colloid Interface Sci*. 2013;407:416–424.
58. Chen D, Holmen A, Sui Z, Zhou X. Carbon mediated catalysis: a review on oxidative dehydrogenation. *Chin J Catal*. 2014;35:824–841.
59. Navalon S, Dhakshinamoorthy A, Alvaro M, Garcia H. Carbocatalysis by graphene-based materials. *Chem Rev*. 2014;114:6179–6212.
60. Kim JY, Lee WH, Suk JW, Potts JR, Chou H, Kholmanov IN, Piner RD, Lee J, Akinwande D, Ruoff RS. Chlorination of reduced graphene oxide enhances the dielectric constant of reduced graphene oxide/polymer composites. *Adv Mater*. 2013;25:2308–2313.
61. Zhang C, Fu L, Liu N, Liu M, Wang Y, Liu Z. Synthesis of nitrogen-doped graphene using embedded carbon and nitrogen sources. *Adv Mater*. 2011;23:1020–1024.
62. Ding W, Wei Z, Chen S, Qi X, Yang T, Hu J, Wang D, Wan LJ, Alvi SF, Li L. Space-confinement-induced synthesis of pyridinic- and pyrrolic-nitrogen-doped graphene for the catalysis of oxygen reduction. *Angew Chem Int Ed*. 2013;52:11755–11759.
63. Wu G, Mack NH, Gao W, Ma S, Zhong R, Han J, Baldwin JK, Zelenay P. Nitrogen-doped graphene-rich catalysts derived from heteroatom polymers for oxygen reduction in nonaqueous lithium-O_2 battery cathodes. *ACS Nano*. 2012;6:9764–9776.
64. Kissin YV. Chemical mechanisms of catalytic cracking over solid acidic catalysts: alkanes and alkenes. *Catal Rev*. 2001;43:85–146.
65. Qi W, Liu W, Zhang B, Gu X, Guo X, Su D. Oxidative dehydrogenation on nanocarbon: identification and quantification of active sites by chemical titration. *Angew Chem Int Ed*. 2013;52:14224–14228.

Manuscript received Jan. 26, 2015, and revision received Apr. 12, 2015.